INFORMATION TO USERS

This manuscript has been reproduced from the microfilm master. UMI films the text directly from the original or copy submitted. Thus, some thesis and dissertation copies are in typewriter face, while others may be from any type of computer printer.

The quality of this reproduction is dependent upon the quality of the copy submitted. Broken or indistinct print, colored or poor quality illustrations and photographs, print bleedthrough, substandard margins, and improper alignment can adversely affect reproduction.

In the unlikely event that the author did not send UMI a complete manuscript and there are missing pages, these will be noted. Also, if unauthorized copyright material had to be removed, a note will indicate the deletion.

Oversize materials (e.g., maps, drawings, charts) are reproduced by sectioning the original, beginning at the upper left-hand corner and continuing from left to right in equal sections with small overlaps.

ProQuest Information and Learning
300 North Zeeb Road, Ann Arbor, MI 48106-1346 USA
800-521-0600

A STUDY OF THE EXCITED STATES IN O^{16} AND Ca^{40} USING 14.1 MeV NEUTRONS

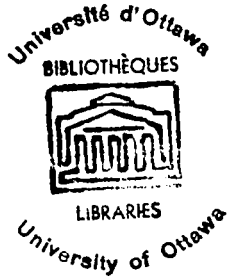

by

W. John McDonald

Submitted in partial fulfillment
of the requirements for the degree of
Doctor of Philosophy.

Department of Physics,
Faculty of Pure and Applied Science,
The University of Ottawa,
Ottawa, Canada.

1964

Approved for the

Department of Physics

Supervisor

Chairman of the Examining Committee

Chairman of the Department

ABSTRACT

The $(n,n'\gamma)$ reaction at $E_n = 14.1$ MeV has been studied for O^{16} and Ca^{40}. Differential cross sections were obtained for the scattering by the ground states and several excited states. The excitation of the lowest 3- state was quite strong for each nuclide. This is evidence that the collective octupole description is valid for these 3- states. The elastic cross sections were successfully fitted using the optical model. The optical parameters which resulted were employed in DWB calculations to predict scattering cross sections for the lowest 3- states of O^{16} and Ca^{40}. For these calculations, the 3- states were represented by collective octupole vibrations. The agreement with experiment was good in the case of Ca^{40} but poor in the case of O^{16}. The latter result may be due to the inadequacy of the DWB method for such a light nucleus.

Energy, yield and angular distribution measurements were made for the deexcitation gamma rays. For O^{16} the results were used to deduce excitation cross sections which were in good agreement with the neutron data. It was observed that states higher than the first 3- levels in O^{16} and Ca^{40} seldom decay by direct ground state transitions but rather by cascade events which proceed through the first 3- state.

This result is in accord with the assumption of a collective vibrational nature for these states if it is assumed that some of the higher states are formed on top of the 3- level.

STATEMENT OF ORIGINALITY

In so far as the author is aware, the following parts of the present work are original.

1) Excitation of the lowest 3- state in Ca^{40} using 14.1 MeV neutrons and demonstration of the direct nature of this excitation by the use of a DWB calculation.

2) Comparison of the excitation cross section for the lowest 3- state in O^{16} with a DWB calculation and demonstration of a rough agreement between theory and experiment.

3) Determination of the cross sections for 14.1 MeV neutron excitation of the O^{16} states up to 11 MeV using both neutron and gamma ray yield measurements.

4) Determination of the cross sections for 14.1 MeV neutron excitation of Ca^{40} states up to 7 MeV and the yields for the corresponding deexcitation gamma rays.

5) Measurement of the angular distribution of gamma rays emitted by the lowest 3- states in O^{16} and Ca^{40} following 14.1 MeV neutron scattering.

ACKNOWLEDGEMENTS

I wish to express my appreciation to Dr. J.M. Robson for suggesting the problem and for his advice and guidance without which the work could not have been successful.

The participation of Dr. I.L. Fairweather in the experiment to measure cascade gamma rays from O^{16} and the help of Dr. D. McPherson of Chalk River in performing the optical and DWBA calculations are gratefully acknowledged.

Thanks are also due the faculty and students of the physics department for stimulating discussions, and to the staff for their assistance in clearing up many experimental difficulties.

The receipt of financial assistance in the form of a grant from the province of Ontario is appreciated.

Finally, I would like to thank my wife for her patience and support throughout the course of the work.

TABLE OF CONTENTS

TABLE OF CONTENTS (continued)

LIST OF ILLUSTRATIONS

LIST OF ILLUSTRATIONS (continued)

*Incorrectly marked SBA on the diagram.

LIST OF ILLUSTRATIONS (continued)

LIST OF TABLES

CHAPTER I

INTRODUCTION

a) Object

The energy levels of nuclei are interpreted at the present time by classifying them in two broad groups, the cloud excitations and the core excitations[1]. The core consists of the nucleons in filled shells. In equilibrium it has spherical symmetry and is quite resistant to changes in its configuration. The cloud consists of the extra nucleons (or holes) required to make up the total number of nucleons, A. Such a division follows naturally from the independent particle model, which pictures each nucleon of a nucleus as moving in a potential well that represents the net force of all the other nucleons in the nucleus on that one. With the correct choice of potential this model gives rise to the shell structure of nuclei in which groups of levels called shells are separated from the neighbouring shells by fairly large energy gaps. Thus, a particularly stable configuration (the core) occurs whenever a shell is completely filled. Extra nucleons (or holes) added to the closed shell form a loosely bound and fairly deformable cloud. It is the excitations of the cloud which have been the subject of most nuclear spectroscopic study to date. In the case of a single cloud particle, where particle stands for nucleon or hole, single particle excitations occur. If there are only a few particles in the cloud, residual forces which are not taken into account by the average potential well tend to couple them into pairs

having zero angular momentum. This tends to promote a spherical equilibrium shape for the cloud. However collective vibrations of the whole cloud can occur. They couple, in the case of an odd number of cloud particles, with the spin of the last odd one to form multiplets. If the number of cloud particles is large, the residual forces tend to deform the cloud in its lowest state thus permitting collective rotational excitations to occur. These can also couple with the spin of a last odd particle to form multiplets. The distinguishing feature of all the cloud spectra is a strong dependence on the number of cloud particles and therefore on the magic nucleon numbers at which closed shells occur.

It is interesting to note that both the single particle and collective states arise quite naturally out of the independent particle picture. Formerly it was necessary to postulate two models, the extreme single particle model which was based on the assumption of weak inter-nucleon interactions, and the collective model which required that these same inter-nucleon interactions be so strong, that the nucleus could be thought of as a drop of liquid. The apparent contradiction of these two models is resolved by the independent particle model.

There has been much interest recently in the core excitations, which are distinguished by a smooth variation with atomic number independent of shell closure. The giant dipole resonance which occurs for all nuclei at an excitation of about 20 MeV is interpreted as a core state in which all the neutrons vibrate collectively against all the protons. In addition there is convincing evidence for a collective octupole vibration of the core at an excitation energy of

about 3 MeV in many nuclei[2] and a little indirect evidence for a quadrupole vibration at about 12 MeV[3].

The purpose of the present work was to investigate the existence and properties of the octupole vibration in the two closed shell nuclei O^{16} and Ca^{40} using inelastic scattering of 14 MeV neutrons to produce the excitation. These two nuclei are doubly closed shell cores upon which many light and medium weight nuclei are built, and hence any collective vibrations which they exhibit are of importance in understanding the spectroscopy of a whole series of light and medium weight nuclei.

Ca^{40} has a state at 3.73 MeV of the proper spin and parity (3-) which appears to conform to the octupole vibration picture[2]. It was hoped that the present investigation would help to confirm this and would provide additional facts concerning the nature of the octupole vibration.

O^{16} also has a 3- state which has been discussed in terms of the octupole vibration[2] at 6.13 MeV. However it is a very light nucleus having only 16 nucleons, and the replacement of these nucleons by an incompressible fluid which is necessary for the collective model description of an octupole state may be a bad assumption. However collective correlations do occur in the motions of nucleons in light nuclei as evidenced by the whole spectrum of rotational states uncovered in Ne^{20} by Litherland et al[4]. Progress has been made in understanding these correlations within the framework of the independent particle model by using the symmetry properties of the group SU3 to choose from the large number of possible states which

can be built using single particle wave functions, those which have the greatest spatial symmetry to represent the low lying states of the actual nucleus[5]. It is to be hoped that such an approach may permit the description of an octupole-like state in light nuclei within the framework of the independent particle model. In any event the properties of the lowest 3- state in O^{16} require close investigation in order that the predictions of the various theories can be tested.

b) Method

The mechanism which has been used in the present case to excite states in O^{16} and Ca^{40} is the inelastic scattering process using 14.1 MeV neutrons. The usefulness of this process is emphasized by a phenomenon observed by Cohen for inelastic proton scattering[6] whereby energetic nucleons preferentially excite those nuclear states which have a collective nature through direct interactions with the nuclear surface. Pinkston and Satchler[7] have shown that this result is in agreement with the prediction of the distorted wave Born (DWB) theory of direct interaction (DI) inelastic scattering. They were able to show that the spin independent part of the matrix element for DI scattering is closely analogous to the matrix element for an electric multipole transition. Thus the same states which show collective enhancement in the transition rates for gamma ray emission should be strongly excited by DI scattering.

Having found a method of exciting the states of interest, it is necessary to inquire as to what kind of measurements can be made to gain information concerning the nature of these states. First of

all, it is possible to study the excitation process itself by observing the yield, energy, angular distribution and polarization of the scattered neutron. Such data can then be compared with the predictions of DI theories which in general involve some assumptions about the nature of the nuclear states involved in the transition. In this way it may be possible to choose between the various assumptions about the nuclear structure. Second, one can study the decay process whereby the excited nucleus emits some radiation (usually one or more gamma rays) to drop back to the ground state or a stable state of some other nucleus. If higher states than the one under study are excited it may be possible to observe cascade events which proceed through the state of interest. In this case the corresponding transition rates and branching ratios will be of interest since they are in general very sensitive to the nature of the nuclear states involved.

In addition to such separate measurements on the excitation and decay processes it is possible to perform coincidence measurements to observe both processes at the same time. For example the angular correlation of the decay radiation with respect to the scattered neutron could be measured.

In the present investigation the energy, yield and angular distribution of the scattered neutrons and the decay gamma rays have been obtained. The results have been compared with the DI scattering theory. In addition the branching ratio for one of the O^{16} states was measured using a coincidence technique to observe gamma ray cascade events.

c) Nuclear Reaction Models and Direct Inelastic Scattering

Before discussing those theories which are useful in treating direct inelastic scattering of nucleons, it is necessary to have a physical picture of the DI scattering process and some idea of its relation to the other interactions which can occur when an energetic nucleon is incident on a nucleus. To be specific, consider what processes might occur if a nucleon having 10 to 20 MeV of kinetic energy is incident on a nucleus. Such a projectile has a deBroglie wavelength associated with it of 1 to 1.5 fm (10^{-13} cm); that is, of the same order as the nuclear radius which varies between 1 and 10 fm depending on the nucleon number A. One event which has a high probability of occurrence is a simple collision in which the internal state of motion of the nucleus is unchanged (elastic scattering). Classically one might treat such an event in terms of a hard sphere or billiard ball collision, but a more accurate treatment will take into account the wave nature of the nucleon. Then the hard spheres would be replaced by a spherical reflecting surface and an incident plane wave in analogy with the optical mirror and incident plane light wave. The small size of the nuclear mirror relative to the wave length of the nucleon means that diffraction of the wave will be a dominant feature of the scattering.

A second process which is very likely to occur is the absorption of the nucleon to form a compound nucleus. This is a semi stable system. Originally its formation was based on the assumption of strong internucleon interactions which result in a rapid sharing of the kinetic energy of the incident particle with all the nucleons of

the system. It eventually decays when one nucleon or a group of nucleons accidentally obtains enough energy to escape from the region of interaction. Again an optical analogy is useful to describe compound nucleus formation. If the nucleus is thought of as a black (absorbing) sphere, diffraction will still occur to account for the elastic scattering. However that part of the wave which actually strikes the nucleus is now absorbed to form the compound nucleus. Actually the nucleus is only "grey" or partially absorbing for energetic nucleons. For example 15 MeV nucleons are thought to have a mean free path inside a nucleus of the order of 4 fm[8]. This fact has led to the development of the cloudy crystal ball or optical model of nuclear reactions[9] which pictures the nucleus as a potential well in conformity with the independent particle model but includes an absorbing term in the potential to account for compound nucleus formation.

A third possibility is that a reaction will occur in one step without the formation of a compound nucleus. Such reactions are called direct interaction (DI) processes. They include knock on and exchange reactions in which the projectile interacts with a nucleon or a group of nucleons in the nucleus and either the incident or struck particle is emitted, stripping and pick up reactions in which a composite incident particle loses one of its constituents to the nucleus or vice versa and collective inelastic scattering in which the incident particle interacts with the nucleus as a whole to excite a collective mode of motion. It is worth noting that the elastic scattering by the nuclear potential is just a special case of a DI

process.

The compound nucleus and DI reactions are just as different from each other as are the collective and single particle models of nuclear structure, yet Weisskopf[1] has been able to show that they both follow naturally from the more basic independent particle model in the same way as the structure models do. He suggests that every reaction begins through a direct interaction between the projectile and the nucleus as a whole or one of its constituents. The products of this interaction have a good chance to escape from the region of their mutual interaction. If they do, the result is simply a direct reaction. There may however be a second interaction resulting in a further sharing of the incident kinetic energy and hence a smaller probability of escape for the interaction products. After only a few collisions the escape probability is very low, and the process has a good chance to continue until the incident kinetic energy is shared by all the nucleons of the system. This is compound nucleus formation. It is easy to understand on the basis of this picture of nuclear reactions why the two limiting cases are so useful. If the reaction does not terminate in one step (DI reaction), then the chances are quite good that a compound nucleus will be formed.

d) Direct Interaction Theory

There is no exact treatment for DI reactions. An exact treatment would involve solving the many body problem for the nucleons of the nucleus and the projectile in terms of their basic interactions and would yield a complete solution for the elastic scattering, DI and compound nucleus reactions as well as the reactions of intermediate

type. The very fact that a division of the whole interaction has been made implies approximation. In particular the DI reactions are treated by assuming that only a few of all the possible degrees of freedom of the interacting system need be considered.

Two approximate treatments for DI reactions have been used fairly extensively, the Born and adiabatic approximations. The Born approximation involves the assumption that the DI reactions can be ignored relative to the elastic scattering. This results in a perturbation calculation between elastic scattering channels for each DI reaction. If the wave functions for the elastic scattering channels are approximated by plane waves the plane wave Born (PWB) approximation results. This is a bad approximation because the nuclear potential causes a serious distortion of the incident wave. A better result is obtained if the optical model is used to obtain the elastic scattering wave functions by fitting the elastic scattering data. This approach is called the distorted wave Born (DWB) approximation. Unfortunately, a separate solution must be found for each scattering problem, and the solutions are sufficiently difficult that computer techniques have to be used. However the computer programs are available at some laboratories (for example at Chalk River Nuclear Laboratories, Chalk River, Ontario).

Recently an extension of the optical model and DWB approximation for scattering has been made in which the elastic and inelastic scattering problems are treated simultaneously by solving a set of coupled equations[10,11]. This is called the coupled equation (CE) approximation. It has been found that the DWB model treatment can

give results very similar to those of the CE model, provided it is properly used, even if the inelastic scattering is quite strong[12].

In appendix A it is shown how the PWB, DWB and CE approximations for the DI scattering cross section are obtained from a general scattering Hamiltonian. The method of solution is given for the DWB case and it is shown how the excitation of collective states can be treated. The complete PWB solution for excitation of collective states through a surface interaction is given.

The adiabatic approximation can be used in the case of collective excitations by direct inelastic scattering[13]. It is based on the assumption that the nuclear motions are slow relative to the interaction time. The elastic scattering probability is calculated as a function of a nuclear motion parameter p which is considered fixed for the calculation. The cross section can then be obtained by taking a suitable integral over p. The adiabatic calculation is in general very difficult, and since it has been found to reduce, in the limit of small collective deformation of the nucleus, to the DWB result[14], little attempt has been made to perform accurate adiabatic calculations for inelastic scattering. The chief interest in the method lies in the fact that a useful closed form expression for the scattering can be obtained in the case of a black nucleus using the Fraunhofer approximation for diffraction of light by a black disc. Blair has given a thorough treatment of this simplified adiabatic model[15], and it will be called the Blair Model in this discussion although others initiated and contributed to its development (see reference 15). In the case of inelastic scattering of alpha particles the nucleus is

fairly black. For example, the mean free path for a 22 MeV α particle in a nucleus has been estimated by Igo and Thaler to be about 1.5 fm[16]. Thus it is not surprising that the Blair model works well for alpha particle scattering at least at small angles where the Fraunhofer approximation is valid[14, 15]. For inelastic nucleon scattering the black nucleus assumption is not as good as we have seen, but there is some indication now that crude agreement with experiment can be obtained despite this[17]. The chief importance of the Blair model lies in its emphasis of the role which diffraction plays in the nuclear inelastic scattering processes. This emphasis, which is not evident in the case of the DWB treatment due to the complexity of the calculations, has made it possible to understand better some of the observed characteristics of the scattering. For example, the Blair model explains a phenomenon observed for alpha particle scattering, namely, that diffraction-like oscillations in the inelastic distribution are found to be either in phase or 90° out of phase with the corresponding oscillations of the elastic distribution[15].

The angular distribution of the gamma rays which result from an inelastic scattering process depends, in general, on the way in which the excited state was formed and therefore predicted distributions depend on the reaction model which is used. Thus it is possible to obtain predictions for the angular correlation between the gamma ray and the scattered particle or for the angular distribution of gamma rays with respect to the incident beam direction. Such predictions have been given in closed form by Satchler[18] for the PWB approximation. In addition some angular correlation and distribution predictions

based on the DWB theory have been given[19, 20]. Unfortunately the computer programs required to obtain predictions for a given case are not generally available at the present time.

CHAPTER II

MEASUREMENTS

a) Angular Distribution of Scattered Neutrons

i) Experiment: The angular distribution of scattered neutrons was obtained using an associated particle time of flight technique[21]. A plan view of the apparatus is shown in figure 1. The source of 14.1 MeV neutrons was a generator* which used 100 KeV deuterons to produce t(d,n) α reactions. A coincident beam of these neutrons was defined by observing the associated alpha particles with a scintillation detector. This beam was allowed to strike a scattering target, and the scattered neutrons were detected in a second scintillation detector after they traversed a flight path of about 250 cm. By observing the time interval between detection of the scattered neutron and its associated alpha particle, the velocity (and therefore the energy) of the neutron was obtained.

The alpha detector consisted of a 0.0013 cm thick Ne102 phosphor** coupled by a thin lucite light pipe to a CBS-CL1090 photomultiplier tube. A baffle having a rectangular aperture 1.2 cm wide by 2.3 cm high was placed over the scintillator at a distance of 6.5 cm from the tritium target. Using this apparatus and a 0.4 cm diameter collimator for the

*Manufactured by Texas Nuclear Corporation, Austin, Texas.

**Manufactured by Nuclear Enterprises Ltd., Winnipeg, Manitoba.

Figure 1: Plan view of apparatus used to measure the angular distribution of scattered neutrons. The distances shown are those used for the calcium measurements and were changed for the liquid oxygen measurements (see text).

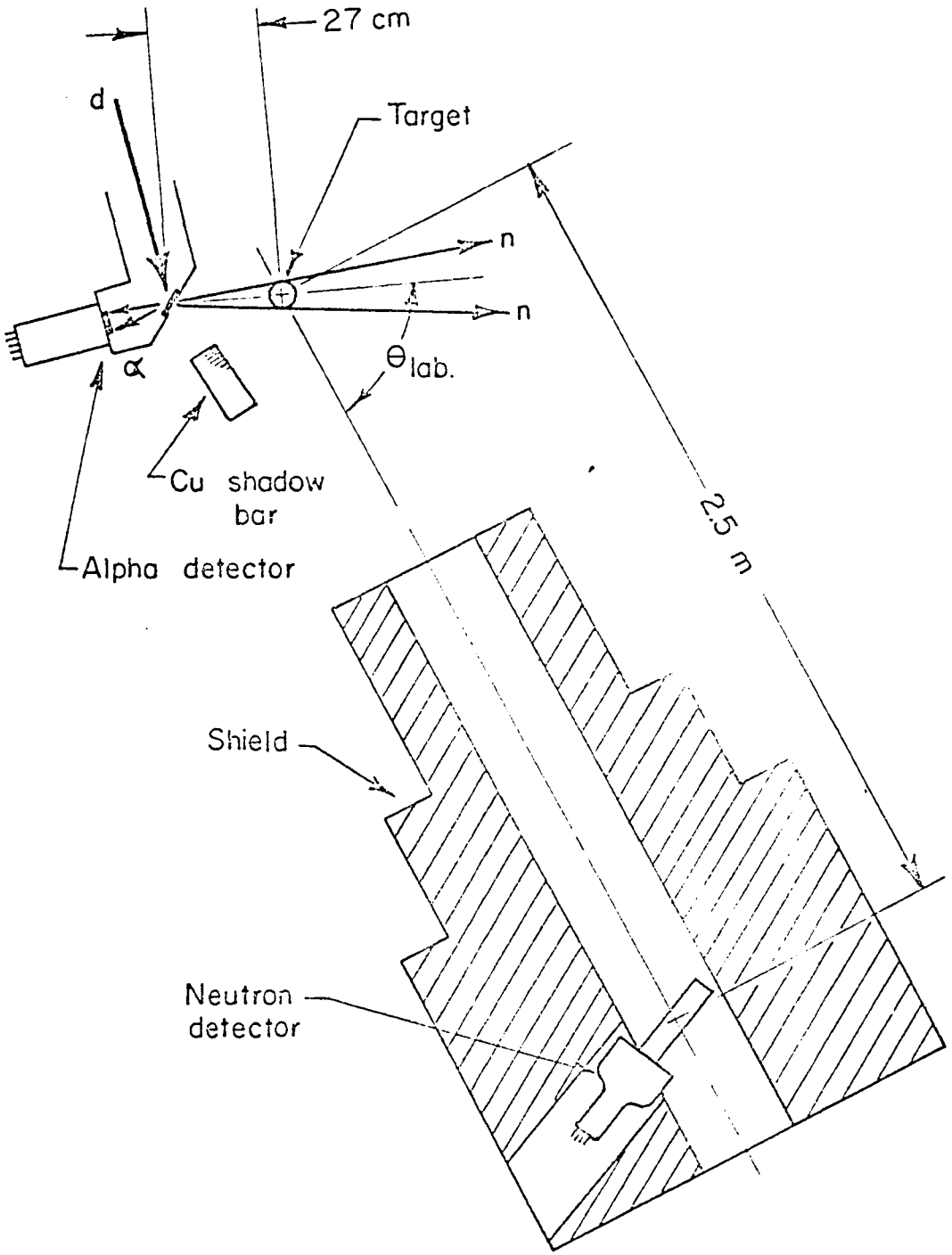
27 cm
d
Target
n
n
α
θlab.
Cu shadow bar
Alpha detector
2.5 m
Shield
Neutron detector

deuteron beam, a rectangular coincident neutron beam was obtained. The vertical and horizontal profiles of this beam are shown in figure 2. They were observed by using a small plastic scintillation probe and demanding a coincidence with the alpha detector output. The rectangular beam geometry was useful in two ways. First, it was possible to irradiate the scattering target fairly uniformly without having large numbers of coincident neutrons going around the target into the room. Thus the probability for observing spurious coincident events was lowered. Second, in the case of oxygen measurement a liquid oxygen target was used, and since the level of the liquid was difficult to maintain at a constant value, it was allowed to vary, but outside the upper limit of the coincident beam (see the arrows marked O-O in figure 2). Thus the edge of the beam itself was used as the effective upper limit of the scattering target.

The neutron detector used for the oxygen measurement consisted of an Ne102 plastic phosphor 5 in diameter by 5 in long with its axis parallel to the flight path and mounted on an RCA7046 photo-multiplier tube. Before the calcium measurement was made the cylindrical phosphor was replaced with an Ne102 slab 4 in by 2 in by 12 in placed at an angle to the flight path as shown in figure 1. This replacement was made in order to improve the time resolution of the system. By adjusting the angle which the slab made with the flight path, it was possible to arrange that the total of the flight time and light collection time was a constant for different points along the slab[22].

Figure 2: Horizontal and vertical plane profiles of the coincident neutron beam. The arrows ()-() indicate the position of the liquid oxygen target.

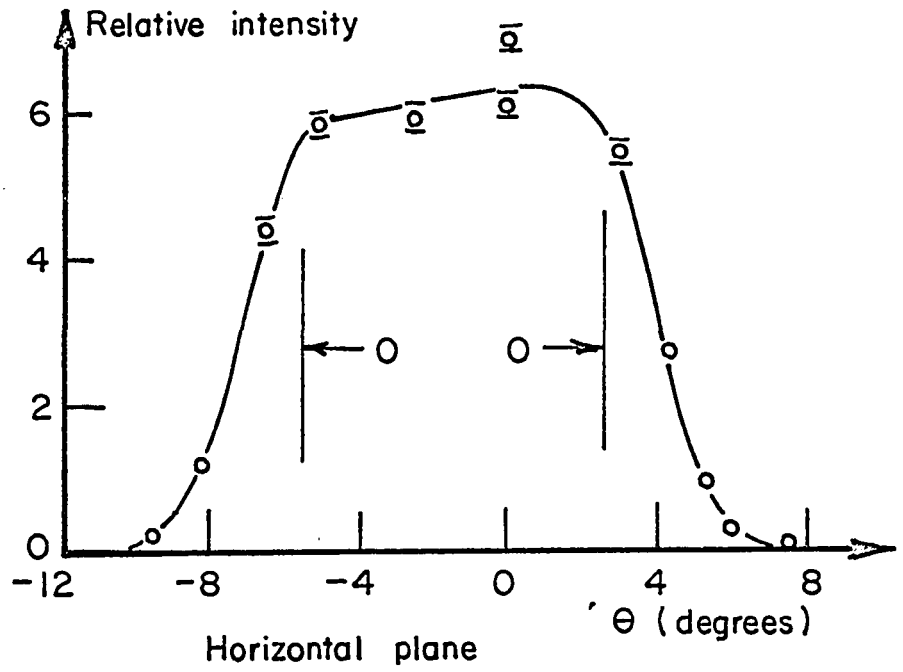

Horizontal plane

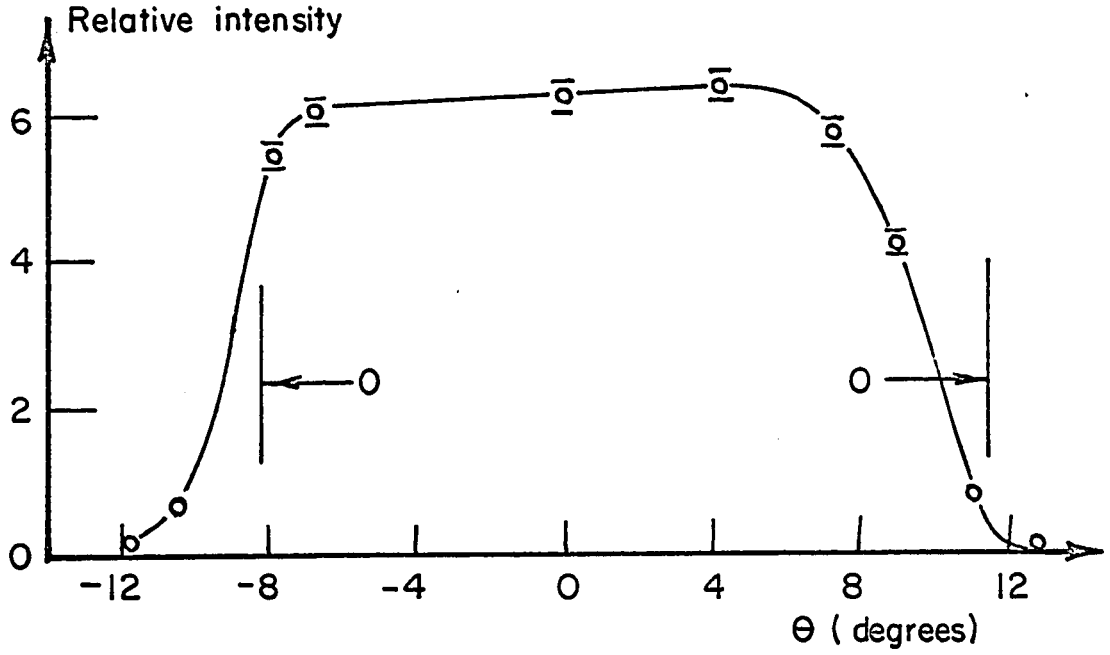

Vertical plane

Liquid oxygen (99.76% O^{16}) was used as the scattering target for the oxygen measurement. It was contained in a thin walled styrofoam vessel. The level of the liquid was maintained automatically through the action of a float operated valve. The effective dimensions of the target were 8.9 cm diameter by 20.6 cm high, and it was placed 65 cm from the neutron source. The angular resolution which was obtained under these conditions was about 11 degrees. For the calcium measurement, a metallic calcium target was used (96.96% Ca^{40}). The dimensions of this target were 4.88 cm diameter by 10.59 cm long, and it was placed 27 cm from the neutron source. The angular resolution obtained using this target was about 10 degrees.

A limitation to the sensitivity of time of flight measurements is imposed by the occurrence of chance coincidence events as a result of the detection of background radiation in the two detectors. In the present case it was possible to ensure that nearly all the signals from the alpha detector which were used were due to the detection of alpha particles simply by using a single channel analyser to select pulses having the proper amplitude.

Pulse height selection was of little value in the case of the neutron detector pulses since monoenergetic neutrons produce pulses having a wide variety of amplitudes[22]. In addition the background counting rate in the neutron detector is generally high as a result of neutron radiation coming directly from the neutron source, neutron scattering by the walls of the room, gamma ray production resulting from neutron capture events in the walls of the room and natural background radiation. Thus it was advantageous to shield the neutron

detector from the radiations coming from sources other than the scattering target as well as possible. Brief tests concerning the effectiveness of various shielding materials and configurations resulted in the choice of the following arrangement. A copper shadow bar (about 25 cm in length) was placed between the detector and the neutron source to shield the detector from direct irradiation. In addition, a castle of masonite and steel blocks about 25 cm thick and lined with 5 cm of lead was constructed around the detector. A snout extending out from the detector toward the scattering target helped to shield the detector and the material immediately around it from direct irradiation (see figure 1).

In addition to the random chance coincidence background, there was a non-random source of background in the case of the oxygen measurement due to the presence of the styrofoam container. For this reason background runs were made at each scattering angle with the empty container in place in order that this background could be subtracted.

The measurement of the flight time was accomplished using the electronic apparatus which is depicted schematically in figure 3. Details of some of the apparatus components are given in the circuit diagrams of appendix C. It should be noted that many modifications to the apparatus were made during the course of the work. The apparatus illustrated in figure 3 and appendix C represents the configuration which was used in the case of the calcium measurements. In the case of the oxygen measurements which were made earlier, tube circuits were used for the preamplifiers and no compensation circuit was employed. These differences affected only the time resolution and chance

Figure 3: Block diagram of the electronic apparatus used in the time of flight measurements. The symbols refer to the following components:

α	alpha detector
n	neutron detector
EF	emitter follower
L	limiting preamplifier
TAC	time to amplitude converter
K	clipper circuit
FC	fast coincidence circuit
A	amplifier
SCA	single channel analyser
C	compensation circuit
TC	triple coincidence circuit
MCA	multichannel analyser.

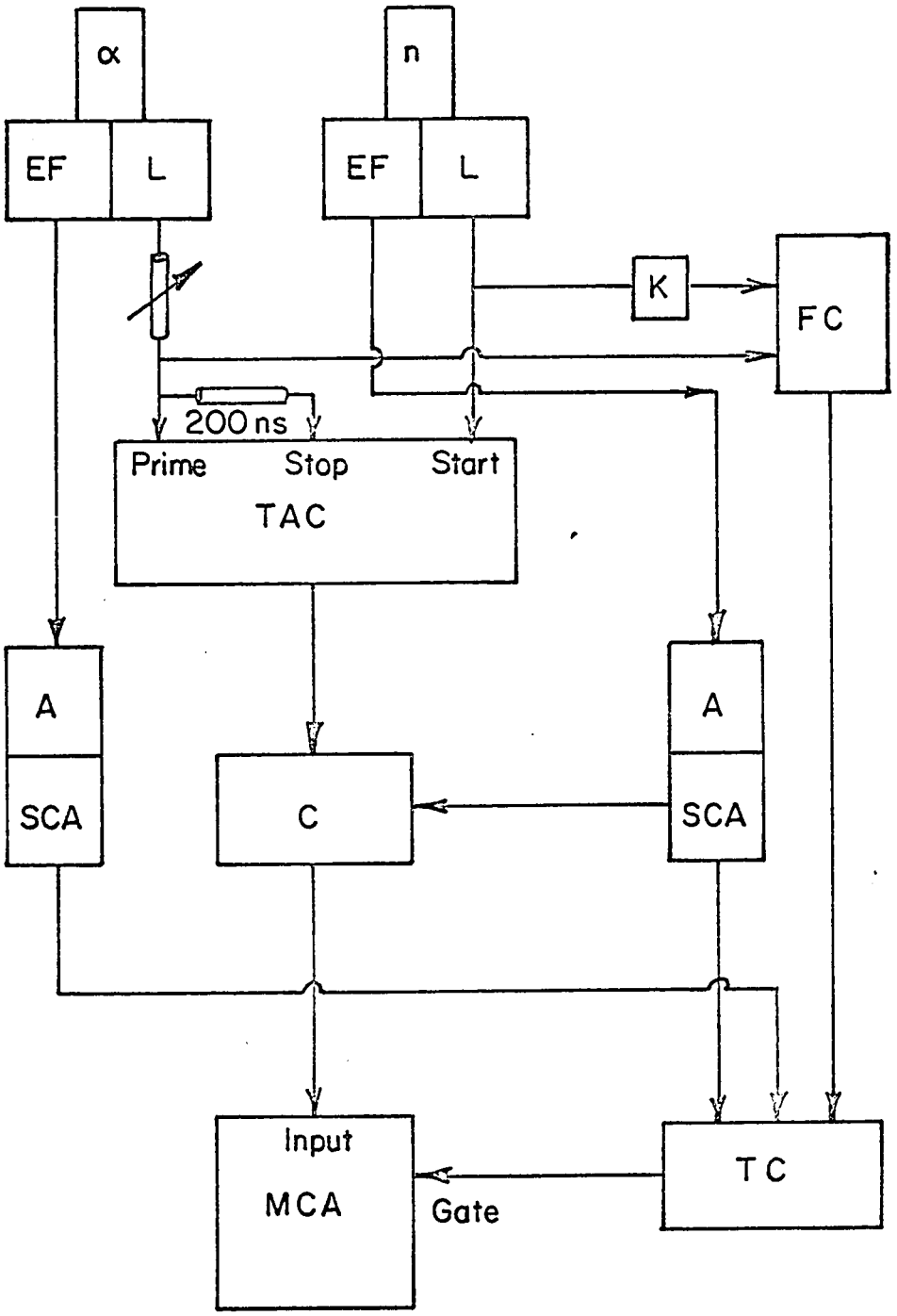
α
n
EF
L
EF
L
K
FC
200 ns
Prime
Stop
Start
TAC
A
SCA
C
A
SCA
Input
MCA
Gate
TC

coincidence counting rates as will be seen below.

The principle of operation of the apparatus was as follows. Fast rising pulses from the limiting preamplifiers were applied to the prime and stop inputs of a time to pulse height converter (TAC) after adjusting the delays so that the earliest neutron pulse just followed the corresponding alpha pulse. The designs for the TAC circuit, the limiting preamplifiers and the compensation circuit (appendix C) are based on those of Fraser and Tomlinson[23]. The TAC circuit produced an output pulse whose amplitude depended linearly on the time interval between the arrival of a neutron pulse at the start input and that of an alpha pulse, which was delayed by 200 ns (1 ns $=10^{-9}$ s), at the stop input. The neutron detector was used to supply the start pulse because it had the lower counting rate. The TAC output was applied to a compensation circuit where a small voltage was subtracted from it to correct for the variation in observed flight time of neutrons having the same velocity but which produced scintillation pulses of different amplitudes. This effect was due to the fact that the limiting preamplifiers required a finite current to limit and therefore produced output pulses sooner for large scintillation pulses than for small ones.

Linear side channels, consisting of conventional emitter follower preamplifiers, amplifiers and single channel analysers were used to choose the detector pulses having the desired amplitude. In the case of the alpha detector, this meant putting a window over the alpha peak. For the neutron channel the bias was set as low as possible consistent with obtaining good time resolution.

The compensation voltage mentioned earlier was obtained by attenuating and stretching a pulse from the single channel analyser on the neutron side. The pulse used for this purpose was that part of the linear pulse which was left after the bias voltage was removed. Thus no correction was applied for pulses having amplitudes just greater than the bias voltage, while a correction proportional to the difference between the signal and bias voltage was applied in the case of larger signals.

Pulses from the limiting preamplifiers were also applied to a fast coincidence circuit after clipping the neutron pulse to a length of about 15 ns. In this way it was possible to reject random events for which the start signal did not occur between the prime and stop signals. The function of the prime in the TAC, is to prevent the start pulse from operating the circuit unless there is a stop pulse following. It does not perform the same function as the fast coincidence circuit since it permits the occurrence of random events for which the prime pulse follows the start pulse.

The outputs of the fast coincidence circuit and the two single channel analysers operated a slow triple coincidence circuit (2τ = $2\mu s(10^{-6}$ s)). Time spectra were obtained by applying the compensated time signal to a 200 channel analyser* which was controlled by the output of the triple coincidence circuit.

In order to check the linearity of the time to amplitude

*Model ST200D, manufactured by the Victoreen Instrument Co., Cleveland, Ohio.

conversion and to calibrate the system, the position of the time peak associated with the direct 14.1 MeV neutron beam was observed as a function of the distance between the detector and the neutron source. The linearity was found to be good within the accuracy of the calibration, which was about 2%, over a 200 ns range of time intervals.

The time resolution of the system was measured by observing the time spectrum of neutrons in the coincidence beam. The results, shown in figure 4, indicate clearly the usefulness of the slab detector and the compensation circuit. The resolution Δ expressed as a full width at half maximum was found to be 2.5 ns for the slab and 3.2 ns for the cylindrical phosphor when the compensation was adjusted to minimize Δ. For these measurements the bias on the neutron side was adjusted to correspond to the centre of the full energy peak in the pulse height spectrum of the 0.662 MeV gamma rays from a Cs^{137} source. According to the results of Gettner and Selove[24], this bias corresponds to the maximum pulse height for neutrons of 2 MeV.

The efficiency of the alpha detector was assumed to be 100% and counting losses in the alpha channel were ignored. No error results from this assumption because those neutrons associated with lost alpha events were not part of the coincident beam.

The efficiency of each neutron detector was obtained as follows. The direct coincident beam was used to obtain the efficiencies for detecting 14.1 MeV neutrons. To do this the detector was simply placed in the beam and a time spectrum taken. From the ratio of the counts in the time peak to the corresponding number of alpha events and the known cross section of the beam, the efficiency was calculated. For neutrons of other energies the efficiency was measured by comparing

Figure 4: Time resolution of the system for the two neutron detector phosphors used. The compensation circuit has been used to obtain the spectra on the right.

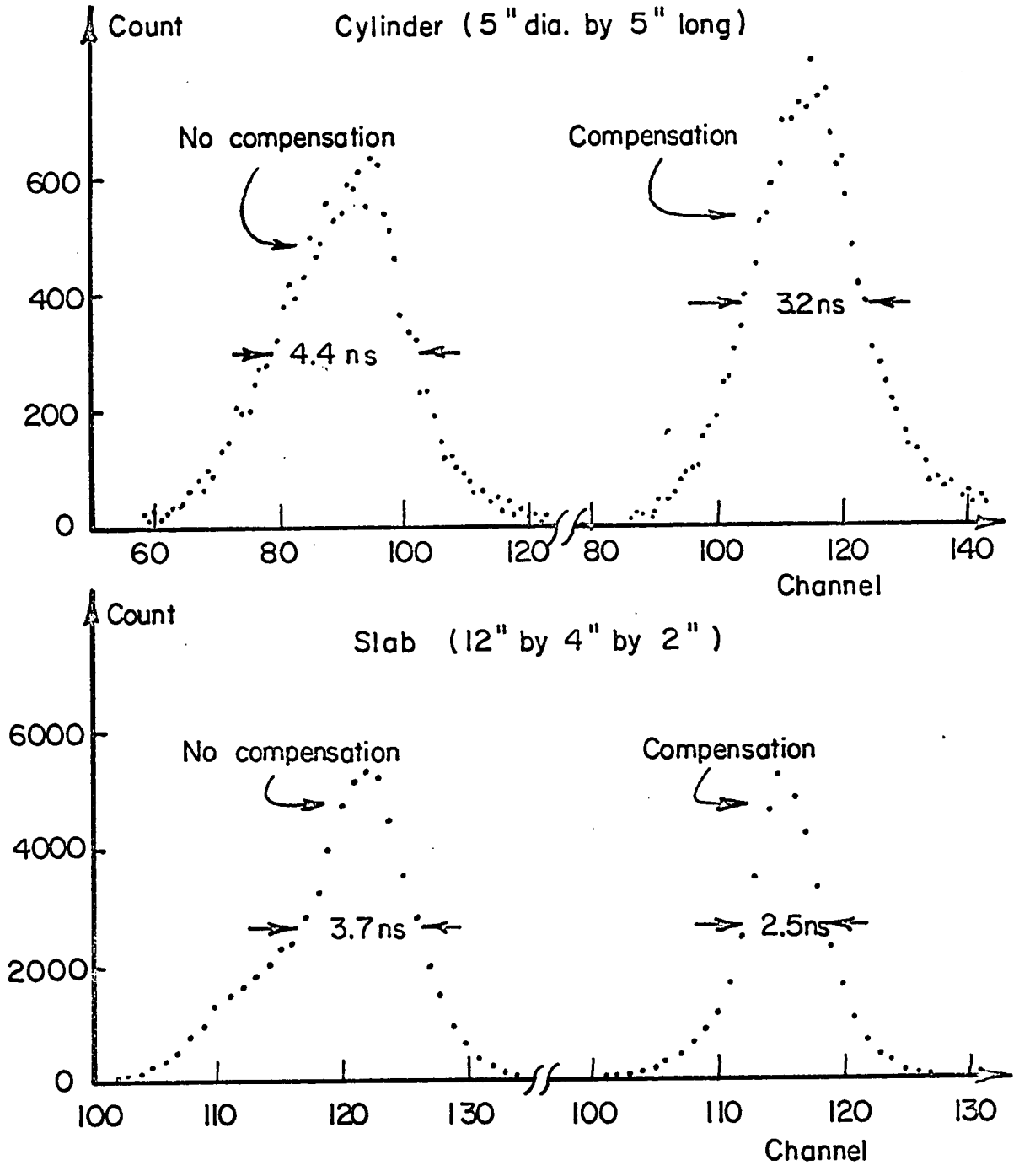
Count
Cylinder (5" dia. by 5" long)
No compensation
Compensation
600
400
200
0
4.4 ns
3.2ns
60
80
100
120
80
100
120
140
Channel
Count
Slab (12" by 4" by 2")
6000
4000
2000
0
No compensation
Compensation
3.7ns
2.5ns
100
110
120
130
100
110
120
130
Channel

the observed yield of neutrons scattered by hydrogen with the theoretical yield at various scattering angles. Since n-p scattering is very nearly isotropic in the centre of mass system, the energy and yield can easily be related to the laboratory scattering angle. Small polyethylene scatterers were used for this measurement. Neutrons scattered by carbon were usually well separated from those scattered by hydrogen in the time of flight spectra. However, in a few cases a correction had to be made for inelastic scattering from the carbon. These corrections were made using time spectra obtained with a graphite scatterer. Corrections were also applied for attenuation of the incident and scattered neutrons by the polyethylene.

The measured efficiencies for the two detectors are shown in figures 5 and 6. Note that the bias of the neutron channel was adjusted to allow detection of neutrons having energies greater than 2 MeV in the cylindrical detector used for the oxygen measurements, while a 3 MeV bias was used with the slab detector for the calcium measurements.

The smooth curves in figures 5 and 6 are theoretical estimates of the efficiencies calculated using hydrogen and carbon cross sections according to the expression given by Rybakov and Siderov[25]. For the experimental points obtained by scattering from hydrogen, the errors indicated in energy represent the energy spread of the scattered neutrons due to the finite angular resolution. The errors in efficiency which are indicated include only relative errors due to statistical and background subtraction uncertainties. The absolute normalization of these data is only accurate to about 10% due to uncertainties in the geometry and the correction for attenuation of the incident neutron

Figure 5: Efficiency of the 5 in diameter by 5 in long Ne102 detector. The curve is theoretical (see text).

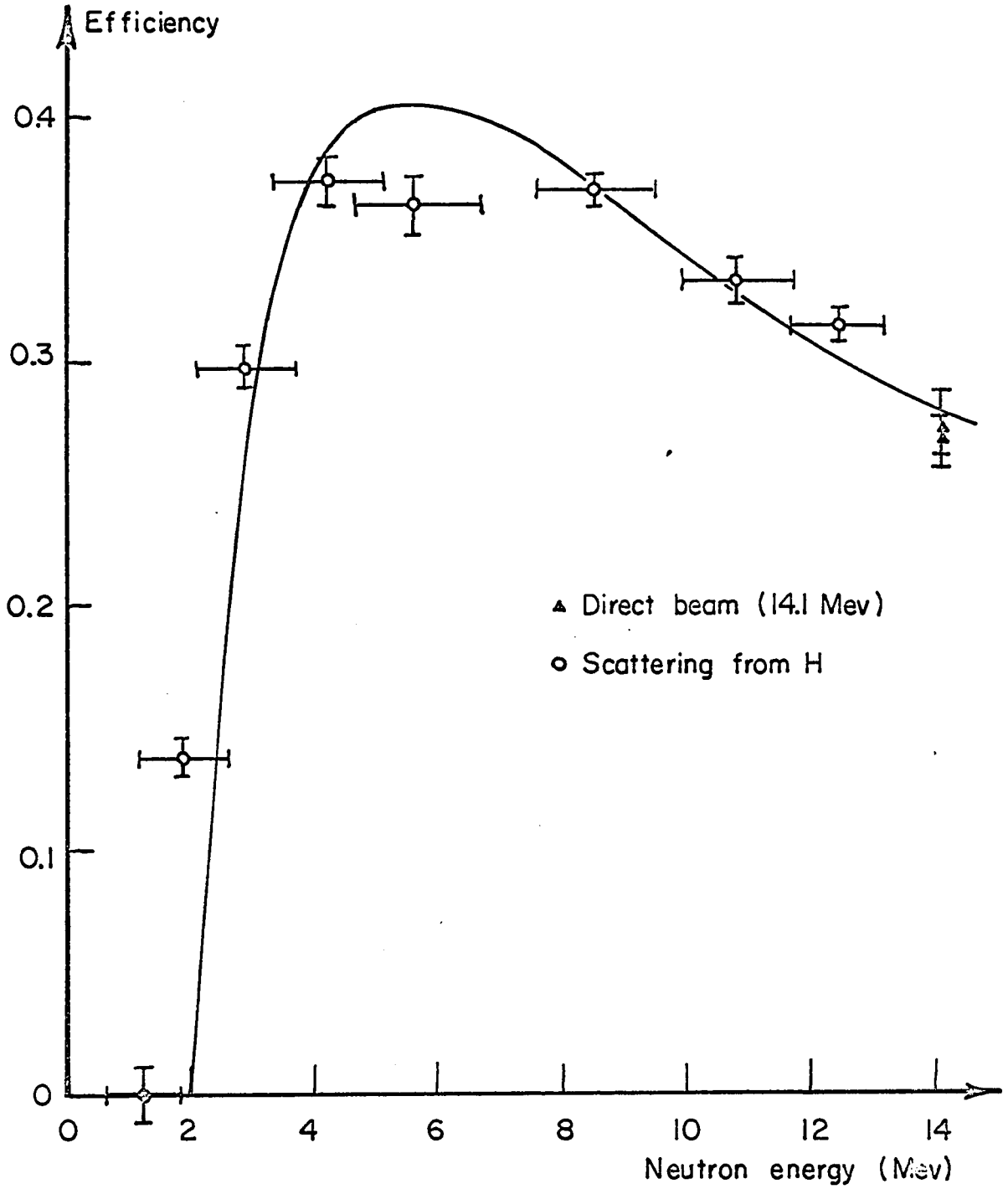
Efficiency
0.4
0.3
0.2
0.1
0
0
2
4
6
8
10
12
14
Neutron energy (Mev)
▲ Direct beam (14.1 Mev)
o Scattering from H

Figure 6: Efficiency of the 12 in by 4 in by 2 in Ne102 detector. The curve is theoretical (see text).

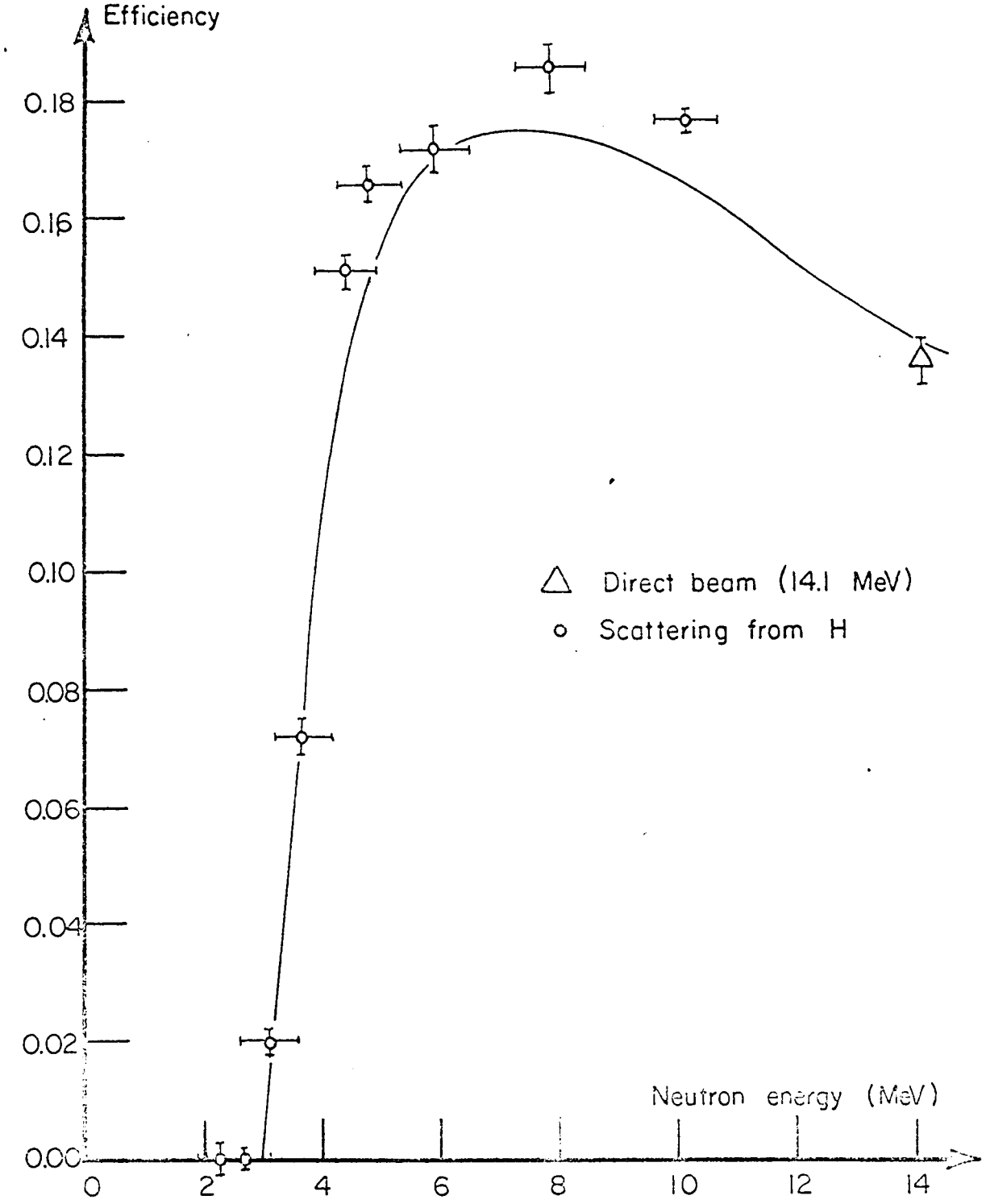
Efficiency
0.18
0.16
0.14
0.12
0.10
0.08
0.06
0.04
0.02
0.00
0
2
4
6
8
10
12
14
Neutron energy (MeV)
Direct beam (14.1 MeV)
Scattering from H

beam. The errors shown for the 14.1 MeV efficiency include the probable error in normalization for the direct beam measurement. Thus, the agreement between the calculated and measured efficiencies is quite good.

ii) Results: A time of flight spectrum of neutrons scattered by oxygen through an angle of 40.3 degrees in the centre of mass system is shown in figure 7. The time increases from right to left and is proportional to the channel number. The gamma ray peak represents the arrival time of the gamma rays which are emitted when the levels excited by the inelastic scattering decay. Elastically scattered 14 MeV neutrons travel at about 1/6 of the speed of light and therefore arrive some time after the gamma rays. The inelastically scattered neutrons arrive still later. The relative positions of the gamma ray and elastic neutron peaks provided a sensitive calibration of the time of flight system which was in good agreement with, but more precise than, the previous determination. This more accurate calibration was used to calculate Q values corresponding to the observed peaks as indicated in figure 7. An energy level diagram for O^{16}, taken from a publication by Bromley et al[26] is included in figure 7.

There is evidence in the time spectrum of fairly strong scattering by at least one of the states near 6.1 MeV, at least one of the states near 7 MeV and by the 2- state at 8.87 MeV. In addition there was some evidence of weak excitation of a state or states at an energy of roughly 11 MeV. The broad peak at channel 90 was split into two components by assuming that only two states were responsible, one at 6.1 MeV and the other at 7 MeV. In order to accomplish this, it was

Figure 7: Time of flight spectrum for liquid oxygen target. Time increases from right to left. 10 channels corresponds to 6.8 ns. The dashed line represents the background which was obtained with no liquid oxygen in the container. The level scheme is taken from reference 26).

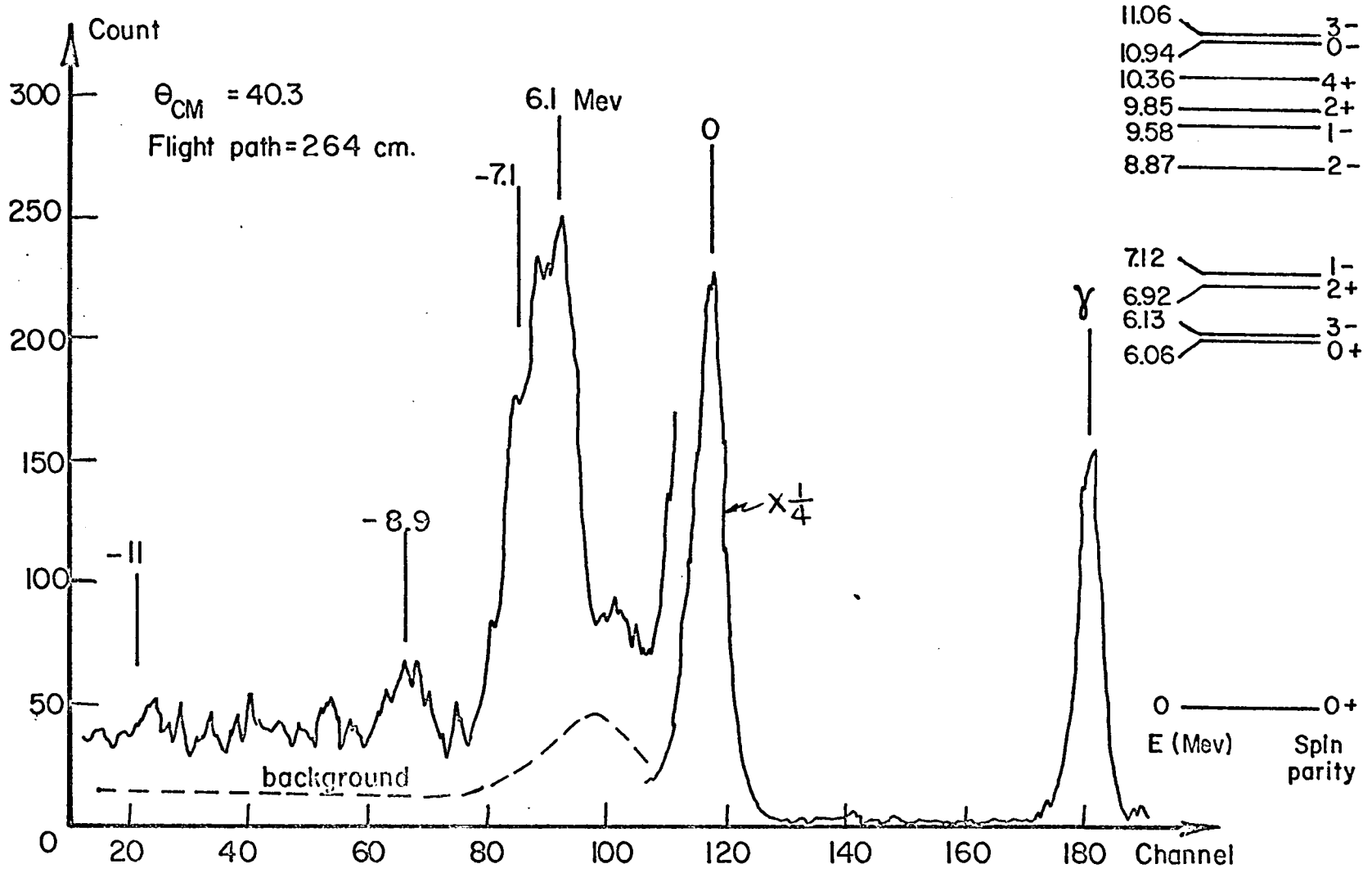
Count
300
250
200
150
100
50
0
θ_{CM} = 40.3
Flight path = 264 cm.
6.1 Mev
-7.1
0
-11
-8.9
X 1/4
γ
background
20
40
60
80
100
120
140
160
180
Channel
11.06
10.94
10.36
9.85
9.58
8.87
3-
0-
4+
2+
1-
2-
7.12
6.92
6.13
6.06
1-
2+
3-
0+
0
0+
E (Mev)
Spin parity

necessary to know the expected shapes of the time spectra due to monoenergetic neutrons of the appropriate energies. These were estimated from the direct beam spectra which had been obtained earlier and from the observed widths of the elastic and 8.87 MeV peaks in figure 7. The latter peaks were used because they were believed to be due to monoenergetic neutrons.

Differential scattering cross sections were calculated from time of flight data like that of figure 7 taken at scattering angles between 15 and 160 degrees. Corrections were applied to account for attenuation of the incident and scattered neutrons. The elastic scattering data were also corrected for the effects of finite angular resolution and multiple scattering by using a Monte Carlo computer program developed by C. Glavina[27]. The Monte Carlo corrections were of the order of 10% or less except near the minima of the distribution, where they were less than 25%.

No angular resolution or multiple scattering corrections were applied to the inelastic scattering data. Errors resulting from this omission should be small since the inelastic scattering cross sections generally do not vary rapidly with angle.

The corrected elastic differential cross section values are plotted in figure 8 as circled points. The inelastic data are plotted as dots with error indication bars. The errors indicated include statistical and background subtraction uncertainties only. They do not include possible errors of 10% for the 6.1 MeV scattering and 20% for the 7 MeV scattering due to the uncertainty in resolving the corresponding peaks. For the elastic cross section values the statistical and background errors were smaller than the diameter of the circles around the points.

Figure 8: Differential cross sections for neutrons scattered by liquid oxygen. The upper curve represents the optical model fit to the elastic data. The other curves simply join sets of points.

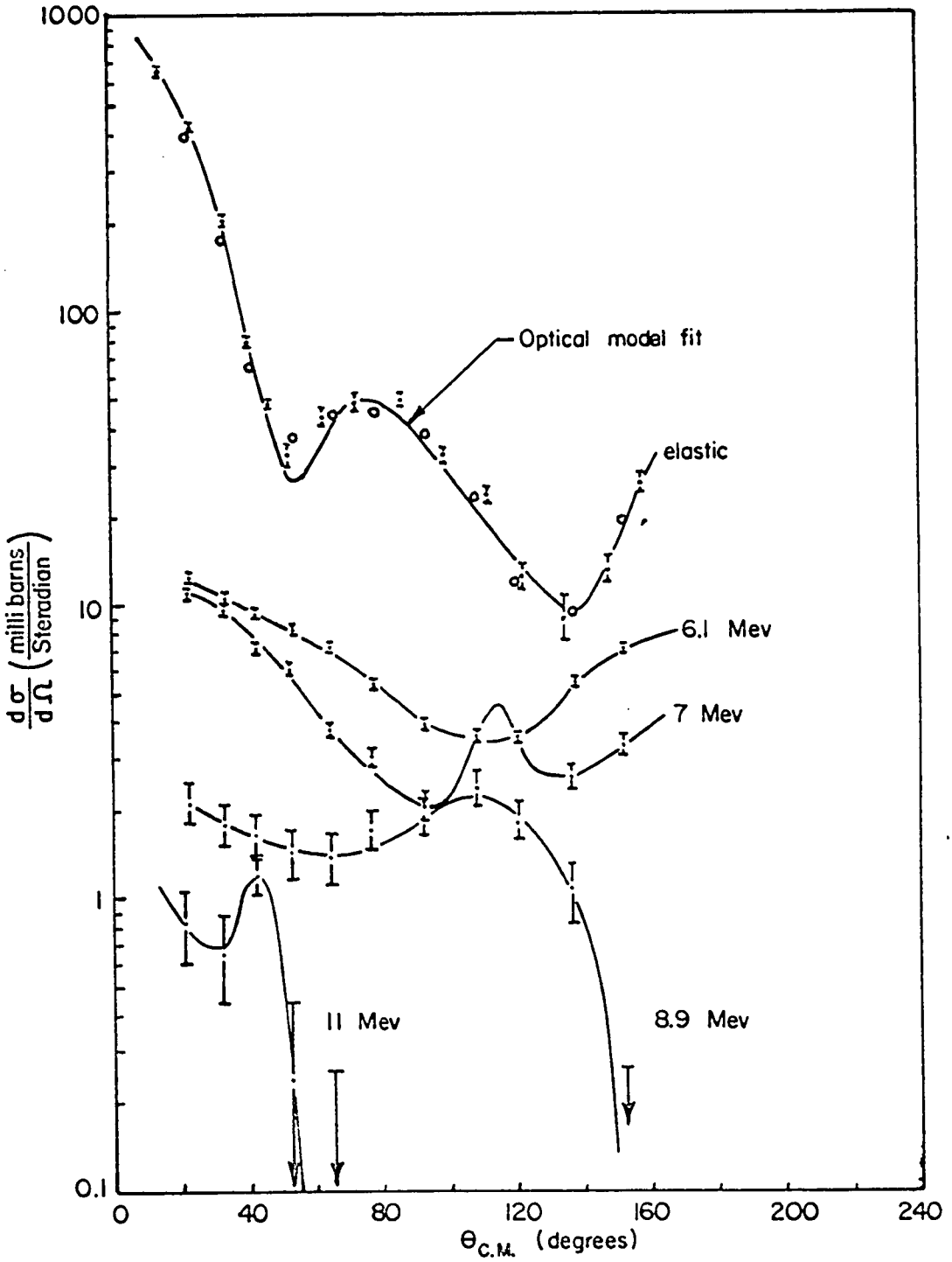
1000
100
10
1
0.1
0
40
80
120
160
200
240
$\frac{d\sigma}{d\Omega}$ ($\frac{\text{milli barns}}{\text{Steradian}}$)
$\theta_{C.M.}$ (degrees)
Optical model fit
elastic
6.1 Mev
7 Mev
11 Mev
8.9 Mev

In addition to the errors indicated there was an uncertainty in the relative cross section for each point of 5% or less due to variations in the sample position, neutron beam cross section, and errors in the Monte Carlo corrections. The absolute value of the integrated elastic cross section, found by drawing a smooth curve (not shown) through the circled points, was 1.07 ± 0.25 b(10^{-24} cm^2). The uncertainty in this quantity was due to uncertainties in the observed cross section of the neutron beam, the location of the scattering target in the beam, the detector efficiency and the attenuation corrections. Because of this large error, the differential cross section values were normalized by setting the integrated elastic cross section equal to 0.87 b, which is the difference between the previously measured total and non-elastic cross sections for 14 MeV neutrons incident on Oxygen[28,29,31] (see table I).

In order to check the accuracy of the differential cross sections, the angular distribution of the elastically scattered neutrons was remeasured using a small scattering target of aluminum oxide powder (Al_2O_3), 3.02 cm in diameter by 6.02 cm long contained in a light cardboard holder. The size of this target ensured that the attenuation corrections would be small and the multiple scattering and angular resolution corrections negligible. Contributions to the elastic time peak due to scattering from the holder and from aluminum nuclei were estimated by performing background runs using a target of rolled aluminum foil in an identical cardboard holder. The foil was rolled so as to produce the same attenuation of the neutrons as did the Al_2O_3 scatterer.

The differential cross section points normalized in the same way as

TABLE I

INTEGRATED CROSS SECTIONS FOR 14.1 MeV NEUTRONS INCIDENT ON O^{16} and Ca^{40}

(in units of 10^{-24} cm^2 (b))

Cross Section	O^{16}		Ca^{40}	
	observed	calculated	observed	calculated
σ_t	1.62 ± 0.04 [28]	1.48	2.24 ± 0.03 [35]	1.95
σ_{ne}	0.75 ± 0.08 [29]*	0.61	1.36 ± 0.02 [29]	1.15
$\sigma_t - \sigma_{ne}$	0.87 ± 0.10	0.87	0.88	0.80
σ_{el}	1.15 ± 0.10 (present work)		0.93 ± 0.10 (present work)	
	1.07 ± 0.25 (present work)		0.82 ± 0.07 [34]	
	0.88 ± 0.09 [30]			

* This quantity has been obtained by adjusting the value of 0.85 b, measured by Flerov and Telyzin[29] using a sphere transmission technique, to account for energy degradation of the elastically scattered neutrons (see the paper by MacGregor et al[31]).

the liquid oxygen data are shown in figure 8 as dots with error indications. The agreement between the two sets of points is good. The present elastic scattering angular distribution and integrated cross section values also agree fairly well with the data of Bauer et al[30].

The integrated cross sections for inelastic scattering based on the same normalization used for the elastic data were as follows:

$Q = -6.1$ MeV $\sigma = 76 \pm 15$ mb

$Q = -7$ MeV $\sigma = 52 \pm 10$ mb

$Q = -8.9$ MeV $\sigma = 18 \pm 5$ mb

Two typical time spectra for neutrons scattered by calcium are shown in figure 9. The peak a in each case corresponds to elastically scattered neutrons. The gamma peak does not appear in the time range covered but would lie to the right beyond channel 200. Using the known time calibration of the system, the peaks b and c were found to correspond to neutrons scattered by states having Q values of -3.7 and -6.7 MeV respectively. A level scheme which gives the known low lying excited states of Ca^{40} is also shown. The data contained in this scheme is taken from Blum et al[32] and from Endt and Van der Leun[33]. Clearly the resolution is insufficient to separate neutrons scattered by the 3- state at 3.73 MeV from those scattered by the 0+, 2+ and 5- states which are nearby. However, the width of the peak b and the low transition probabilities observed for scattering high energy electrons from the 2+ and 5- states[32] suggest small contributions for these states. In the case of the peak c, which was only observed clearly at angles greater than 100 degrees because of background interference, the line width is considerably greater than that of the peaks a

Figure 9: Time of flight spectrum for the calcium metal target. Time increases from right to left. 10 channels correspond to 3.85 ns. The level scheme data has been taken from references 32, 33).

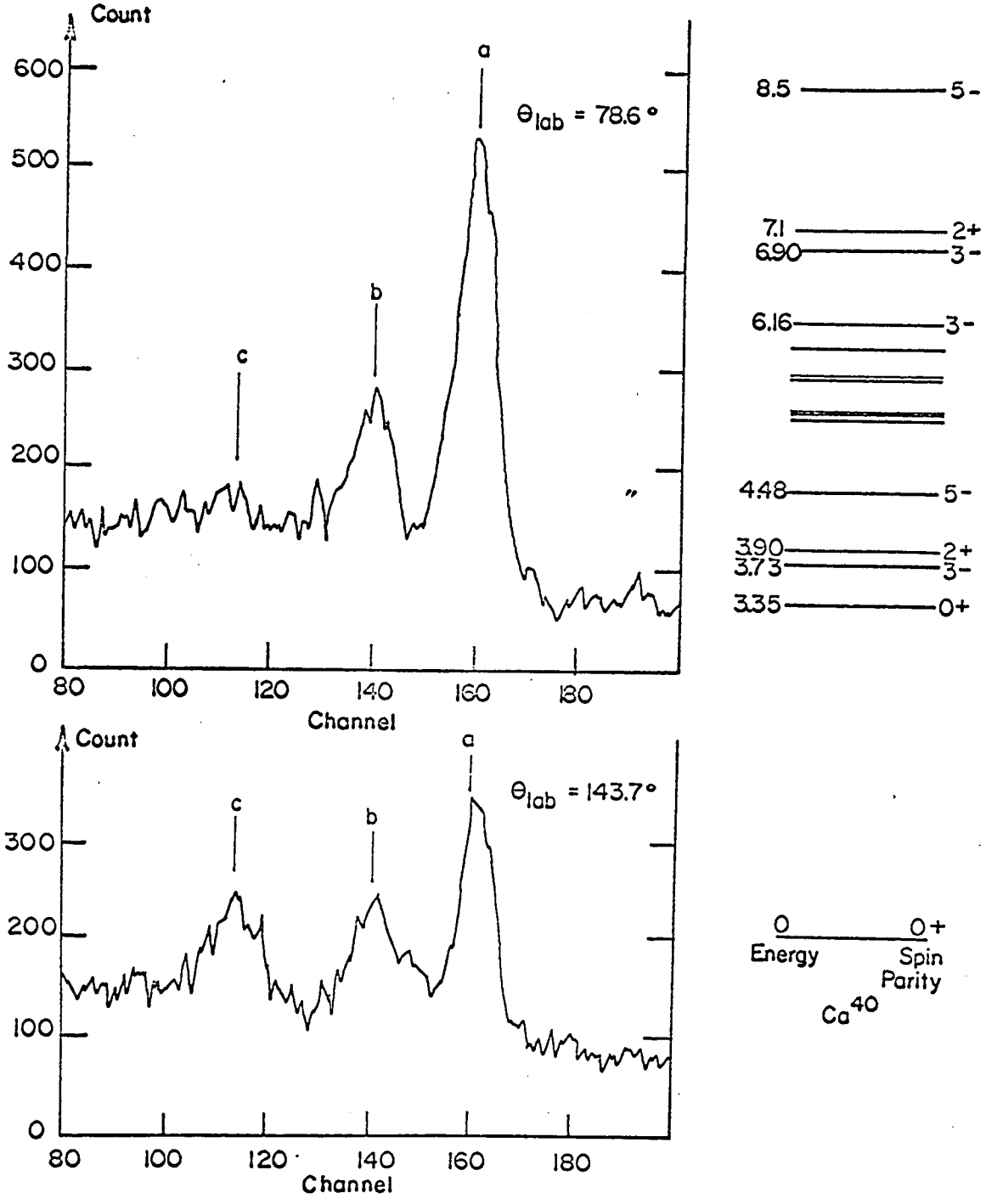
Count
600
500
400
300
200
100
0
80
100
120
140
160
180
Channel
a
b
c
θ_{lab} = 78.6°
Count
300
200
100
0
80
100
120
140
160
180
Channel
a
b
c
θ_{lab} = 143.7°
8.5
5-
7.1
2+
6.90
3-
6.16
3-
4.48
5-
3.90
2+
3.73
3-
3.35
0+
0
0+
Energy
Spin
Parity
Ca^{40}

or b indicating that there might be contributions from more than one state.

Differential scattering cross sections corresponding to the peaks a and b were obtained by collecting time spectra for angles between 20 and 160 degrees. They have been plotted in figure 10. Corrections have been applied to the elastic data for angular resolution and multiple scattering effects using the Monte Carlo method as before. In this case, because of the smaller scattering target, the corrections were only of the order of a few percent except for the points near minima in the distribution where they were sometimes as much as 10%.

The errors indicated for the data of figure 10 include all the known errors in the relative values of the cross section including the statistical, background subtraction, sample position and beam cross section variations, and the Monte Carlo correction uncertainties. The observed angular distribution of elastically scattered neutrons is in good agreement with a previous measurement by Cross and Jarvis[34].

The integrated elastic cross section was estimated in the same way as was done for the oxygen data. The result, $\bar{\sigma}_{el} = 0.93 \pm 0.10$ b, is in good agreement with the difference between the observed total and non-elastic cross sections for 14 MeV neutrons incident on Ca^{40}, which is 0.88 $\pm$ 0.05 b[29,35] (see table I). As in the case of the oxygen data, the differential cross sections shown in figure 10 have been normalized using the latter value. With this normalization, the integrated inelastic scattering cross sections corresponding to the peaks b and c of the time spectra were found to be 43 $\pm$ 10 mb and 20 $\pm$ 15 mb respectively.

Figure 10: Differential scattering cross sections for the calcium metal target corresponding to the peaks a and b of figure 9. The curves have been calculated as described in the text.

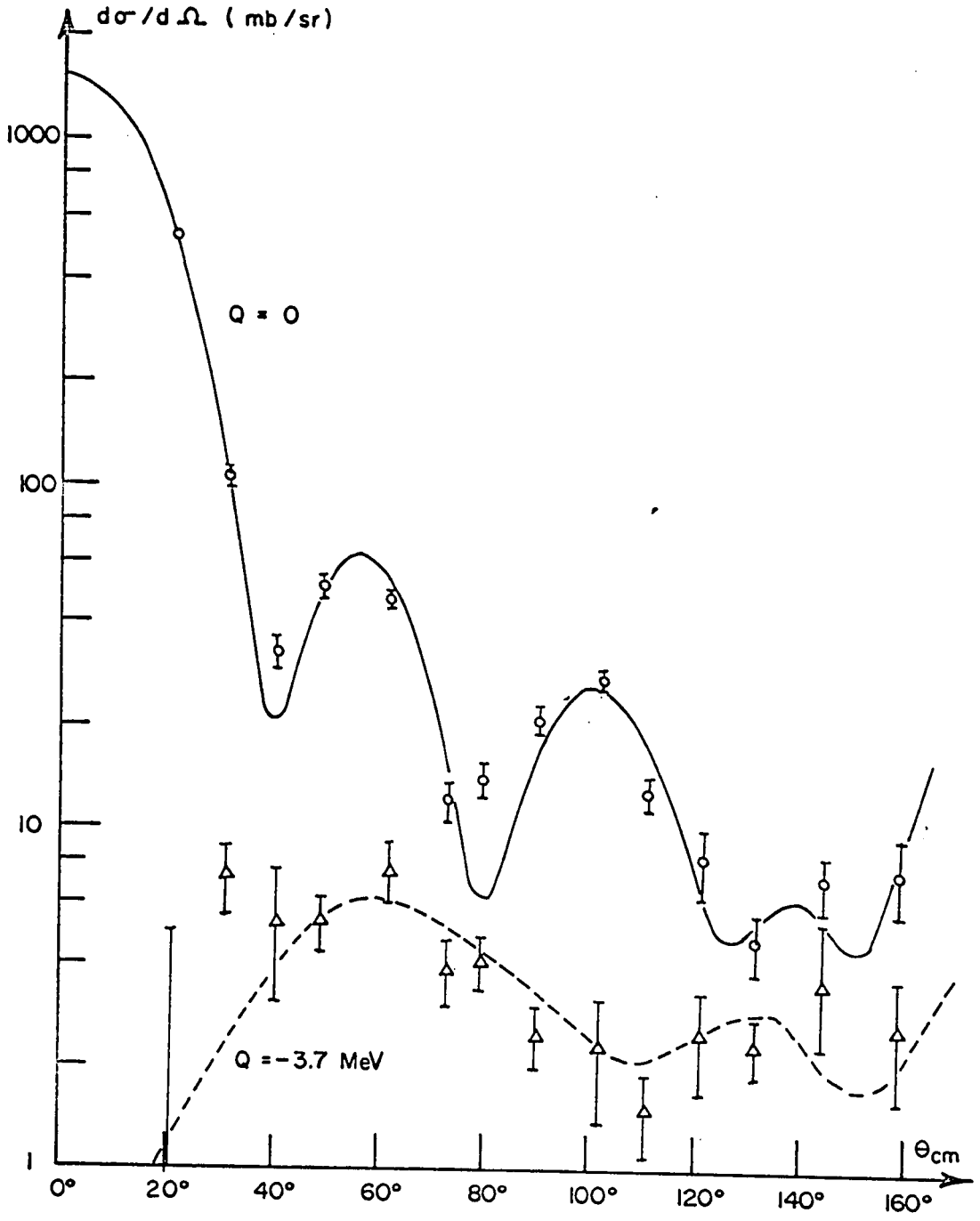
dσ/dΩ (mb/sr)
1000
100
10
1
Q = 0
Q = −3.7 MeV
0°
20°
40°
60°
80°
100°
120°
140°
160°
θcm

iii) Comparison with Theory: The elastic scattering cross sections have been fitted using optical model calculations based on optical potentials of the form

$$V_{OM} = V f(r) + i W_g g(r) + V_s \vec{l}\cdot\vec{s} \left(\frac{\hbar}{m_\pi c}\right)^2 h(r) \qquad (II\,1)$$

where

$$f(r) = \left[1 + \exp\{(r-R)/a\}\right]^{-1},$$

$$g(r) = \exp\left[-(r-R)^2/b^2\right],$$

$$h(r) = \frac{1}{r}\frac{d}{dr}\left[f(r)\right],$$

$$R = R_0 A^{1/3},$$

and A is the atomic number of the scattering nucleus, r is the distance between the projectile and the centre of the nucleus, $\vec{l}$ and $\vec{s}$ are the orbital and spin angular momenta of the projectile, c is the velocity of light and m_π is the mass of a π meson.

The fitting was accomplished using a computer program "Auto prop II" and the Chalk River G20 computer to calculate elastic scattering cross sections for various values of the parameters a, V, W_g, and V_s with b and R_0 fixed. The computer automatically optimised the variable parameters to obtain the closest agreement between the calculated and experimental cross sections. These calculations as well as the DWB and statistical model calculations to be described below were carried out by Dr. D. McPherson using computer programs developed by Drs.

D. McPherson and J.M. Kennedy of Atomic Energy of Canada Ltd., Chalk River, Ontario.

Fits were obtained for three values of the parameter b; 0.8, 1.0, and 1.2 fm with R_0 set equal to 1.25 fm in each case. For the oxygen data, an additional set of fits was obtained with R_0 set equal to 1.2 fm. The choice of optical parameters is somewhat arbitrary as so many of them are used. In order to narrow the choice of optical fits, any result was discarded if it predicted total and non-elastic cross sections that differed greatly from the experimental values given in table I . The best fits which resulted are illustrated by the smooth curves of figures 8 and 10 and the corresponding calculated cross sections of table I. The parameters of the optical potentials which gave these fits are compared in table II with those which other workers have found fit most of the 14 MeV neutron scattering data[36,37]. The two sets of parameters given in the case of O^{16} represent equally good fits. They are included to indicate the extent to which a set of optical model parameters can be altered without changing the fit. The one labelled a has been arbitrarily chosen as the one giving the best fit.

The agreement between the parameters found here and the previous ones is very good except for the spin orbit parameter V_s. The low value obtained in the present case should not be taken too seriously because it is difficult to fix this parameter without measuring the polarization of the scattered neutron.

DWB predictions for inelastic scattering cross sections, corresponding to assumed octupole states at 6.13 MeV in O^{16} and 3.73 MeV in

TABLE II

OPTICAL MODEL PARAMETERS FOR 14 MeV NEUTRONS

Source	Nucleus	R_0 (fm)	a (fm)	b (fm)	V MeV	W_g MeV	V_s MeV	W* MeV
Present work	O^{16}(a)	1.25	0.52	1.0	-47.2	-5.7	-3.0	-
Present work	O^{16}(b)	1.20	0.58	1.2	-49.4	-5.2	-3.2	-
Present work	Ca^{40}	1.25	0.62	1.2	-45.6	-8.2	0	-
Bjorklund and Fernbach[36]		1.25	0.65	0.98	-44	-11	8.3	
Clark and Cross[37]		1.25	0.70	1.10	-44	-7	6	-2

* A volume absorption term $i\,Wf(r)$ has been used by Clarke and Cross[37].

Ca^{40}, have been calculated using the optical parameters which were found in fitting elastic scattering data to define both the incoming and outgoing neutron wave functions (see appendix A). A compound nucleus contribution to the inelastic scattering was estimated in the case of the O^{16} state by using a Hauser-Feshbach statistical calculation to divide up the flux which is absorbed by the imaginary part of the optical potential into all the possible exit channels[38]. In this calculation, the contribution to each channel is weighted according to the optical model transmission coefficient corresponding to that channel. Level densities were required for the nuclides O^{16}, N^{16}, N^{15} and C^{13} which are produced through neutron induced reactions in O^{16}. These were obtained by using known levels and adding a sufficient number of fictitious levels to match the observed level densities for these nuclei[33]. The total inelastic scattering cross section for excitation of all the states in O^{16} by 14.1 MeV neutrons was estimated in this way to be 257 mb. This is close to the sum of the (n,n') cross sections observed in the present work for the 6.1, 7 and 8.9 MeV states plus a probable contribution of about 80 mb for excitation of higher states. (The latter quantity was obtained using (p,p') scattering data for protons having an incident energy near 14 MeV[39].) However the Hauser-Feshbach estimate is based on the assumption that all the inelastic scattering reactions proceed through the compound nucleus stage whereas, in fact, some of the scattering is direct. In particular, the scattering which excites the octupole state is expected to be mainly direct. Therefore the calculated compound inelastic scattering cross sections for excitation of all the O^{16} states σ(calc)

were renormalized to give

$$\overline{\sigma}_{CN} = \overline{\sigma}_{CN}(calc) \left[\overline{\sigma}(6.1) \; / \overline{\sigma}(6.1\,Calc)\right] \quad (II\ 2)$$

where, $\overline{\sigma}_{CN}$ are the normalized compound nucleus inelastic scattering cross sections for all states and $\overline{\sigma}(6.1)$ is the observed scattering cross section corresponding to $Q = -6.1$ MeV. This normalization implies that the scattering by the 6.1 MeV state is entirely direct which is an overestimate. However, since direct contributions to the scattering to the other states have been ignored, the result may be reasonable. Even with this normalization, the estimated compound nucleus contributions to the scattering by individual states can probably be taken as upper limits since the level densities used in the calculation are based on observation and may underestimate the total number of actual levels.

The resulting compound nucleus cross section for excitation of the 6.13 MeV 3- state in O^{16} has been plotted in figure 11 (curve a). No calculation was made of the compound nucleus scattering in the case of the 3.73 MeV 3- state in Ca^{40} because the observed level density is so high that the compound scattering by a single level would be negligibly small.

The inelastic scattering cross section predictions for the assumed octupole states in O^{16} and Ca^{40} are plotted with the experimental data in figures 10 and 11. (It should be noted that the errors indicated for the data of figure 11 include the uncertainty in resolving the 6.1 and 7 MeV peaks of figure 7 as well as the statistical and background subtraction uncertainties.) For O^{16}, two limiting cases have

Figure 11: Comparison of the DWB prediction for scattering by an octupole state at 6.13 MeV in O^{16} with the experimental data ($Q = -6.1$ MeV). Curve c includes no compound nucleus contribution to the scattering. Curve b includes the compound nucleus contribution indicated by curve a.

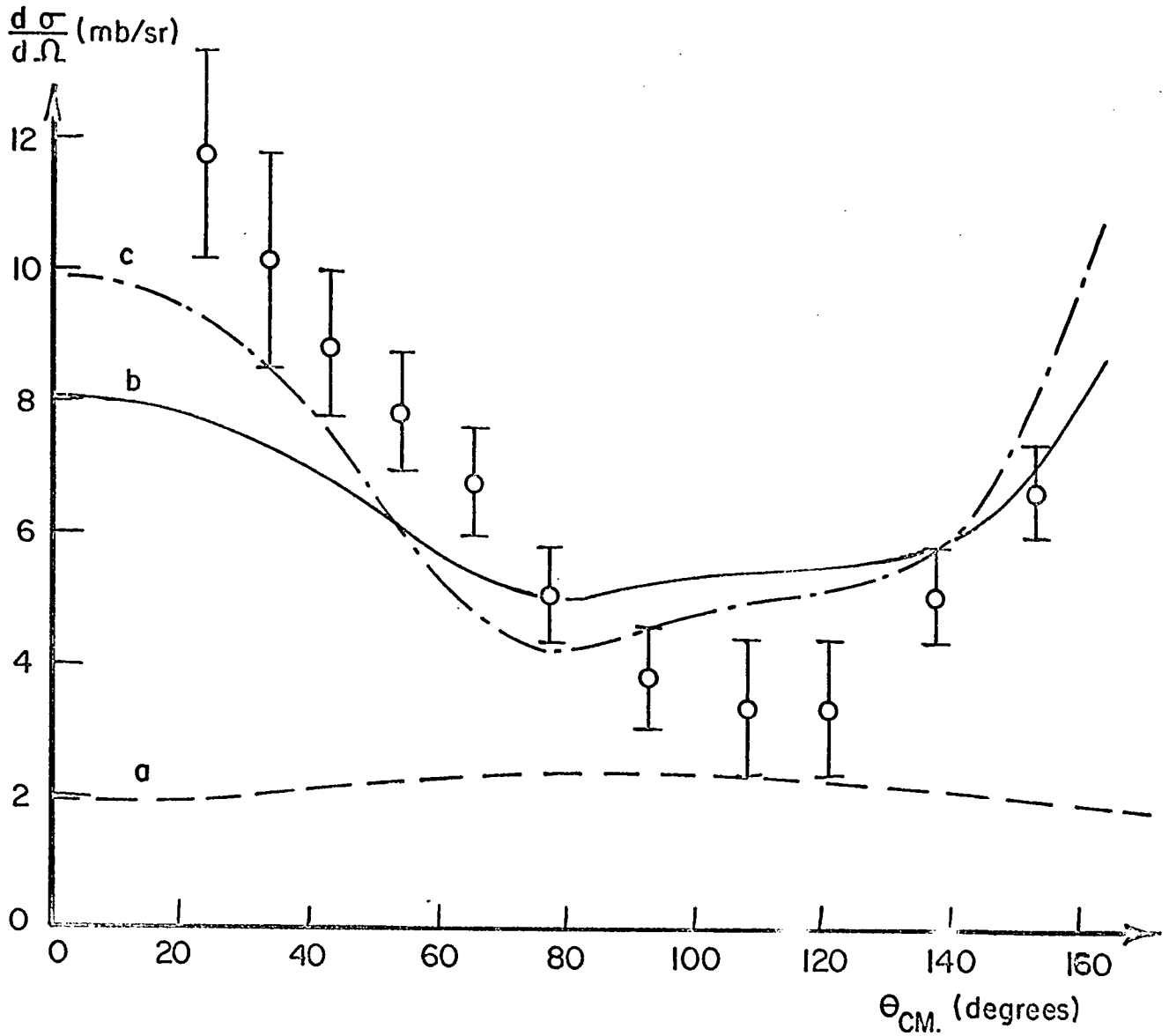
dσ/dΩ (mb/sr)
12
10
8
6
4
2
0
c
b
a
0
20
40
60
80
100
120
140
160
θCM. (degrees)

been plotted, curve b which includes the estimated compound nucleus contribution and curve c which does not. In each case the direct part has been normalized by adjusting a collective model parameter called the rms deformation parameter β_3 (see appendices A and B) to give the same integrated cross section for the sum of direct and compound nucleus contributions as was found experimentally.

The same optical potentials were used to describe the initial and final states of the scattering systems for the DWB calculations because the correct potentials for the final states were not known (appendix A). In order to see if this assumption effected the results, the DWB calculations were repeated with the parameters V and W_g changed in accordance with the expected optical model behaviour[40] to $V + |Q|/2$ and $W_g - |Q|/2$ respectively. Only minor changes in the DWB cross sections resulted. The same was true when alternate sets of optical parameters which gave fairly good fits to the elastic data were tried. In short, good results were obtained for the Ca^{40} scattering ($Q = -3.7$ MeV) for all DWB calculations tried, provided the optical parameters represented a fairly good fit to the elastic data. In the case of O^{16}, the DWB prediction did not agree with the scattering data ($Q = -6.1$ MeV) very well despite the fact that the elastic data were well fitted by the optical calculation.

The values of β_3 deduced from the normalization of the DWB results are compared in table III with estimates of $\beta_3(EM)$ obtained from the mean lifetimes of the excited states as measured using electron scattering[32,41,42,49] and with $\beta_3(SP)$ which corresponds to an extreme single particle lifetime (see appendix B). For O^{16}, two

TABLE III

COLLECTIVE DEFORMATION PARAMETERS FOR O^{16} and Ca^{40}

Nucleus State	Neutron Scattering Calculation	R (fm)	β_3	Electron Scattering β_3(EM)	β_3(SP)
O^{16} 6.13 MeV (3-)	DWB	3.15	0.46(b)	$0.72^{+0.40}_{-0.20}$ [33]	0.20
			0.58(c)		
Ca^{40} 3.73 MeV (3-)	DWB	4.27	0.37	0.35 [41,42]	0.08
	Elair	4.77	0.46	0.29 [32]	
	PWB	6.0	0.035		

values of β_3 have been calculated corresponding to the curves b and c of figure 11 (i.e., b is based on the inclusion of a compound nucleus contribution). The charge distribution which was assumed in order to obtain β_3(EM) was in agreement with that found from electron scattering data[43,44], namely $R_0 = 1.1$ fm and $a = 0.55$ fm, where the form of the distribution is given by $f(r)$ in equation (II 1).

The agreement is good between the values of β_3 deduced from the neutron scattering data and the corresponding values of β_3(EM) in the case of Ca^{40} ($Q = -3.7$ MeV). If there were a compound nucleus contribution to the cross section of 10% (which is almost certainly an overestimate), the value of β_3 would only be reduced by 5%, and the agreement would still be very good. The results for O^{16} ($Q = -6.1$ MeV) are not so easy to compare because there is a large uncertainty in the value of β_3(EM). This uncertainty is due to a large error in the measured mean lifetime and to uncertainty in the shape of the charge distribution. In the case of a light nucleus the latter factor is very important[44]. Comparison of the values of β_3 obtained from the neutron scattering data with the β_3(SP) indicates that there is strong collective enhancement of the transition rates for the 3- states studied.

Glendenning[45] has calculated the inelastic scattering cross section in the DWB approximation for 15 MeV neutrons incident on a hypothetical nucleus having the following parameters:

$$A \simeq 30,$$

$$Q(3^- \text{ state}) = -2 \text{ MeV},$$

$$V = -40 \text{ MeV}, \quad W = -12 \text{ MeV},$$

where the potential used was in the form of a square well

$$V_{SW} = V + iW \quad \text{for } r < R$$

$$= 0 \qquad \text{for } r > R$$

where R = 4.0 fm. He assumed single particle transitions were induced by inelastic scattering at the radius R through a delta function interaction between the projectile and one of the target nucleons. The calculation was found to be fairly insensitive to changes in most of the parameters with the exception of the product VR^2. The above parameters are similar to the optical model parameters for Ca^{40}.

The Glendenning result is compared in figure 12 with the Ca^{40} data (Q = -3.7 MeV). The normalization is arbitrary because this calculation is known to give a poor prediction of the magnitude of the cross section. The agreement is not good. Unless changes in the optical parameters are more important than is suspected, this result suggests that the DWB calculation is sensitive to either the type of nuclear wave function used or to the radial distribution of the interaction. The effect of the nuclear wave functions was investigated by recalculating the Ca^{40} inelastic cross section (Q = -3.7 MeV) for the optical model parameters of the present work, but assuming excitation a particle-hole 3- state by single particle transitions from the closed $d_{3/2}$ shell

$$(d^4_{3/2})_{J=0+} \rightarrow (d^3_{3/2}, f^1_{7/2})_{J=3-}$$

The interactions were allowed to occur throughout the nuclear volume. This calculation was performed by Dr. N.K. Glendenning of the Lawrence Radiation Laboratory, Berkley, California. The shape of the resulting cross section was nearly identical with that calculated using the

Figure 12: Comparison of the observed scattering (Q = -3.7 MeV) for calcium and the Glendenning, Blair and PWB* calculations described in the text.

*incorrectly marked SBA on the diagram.

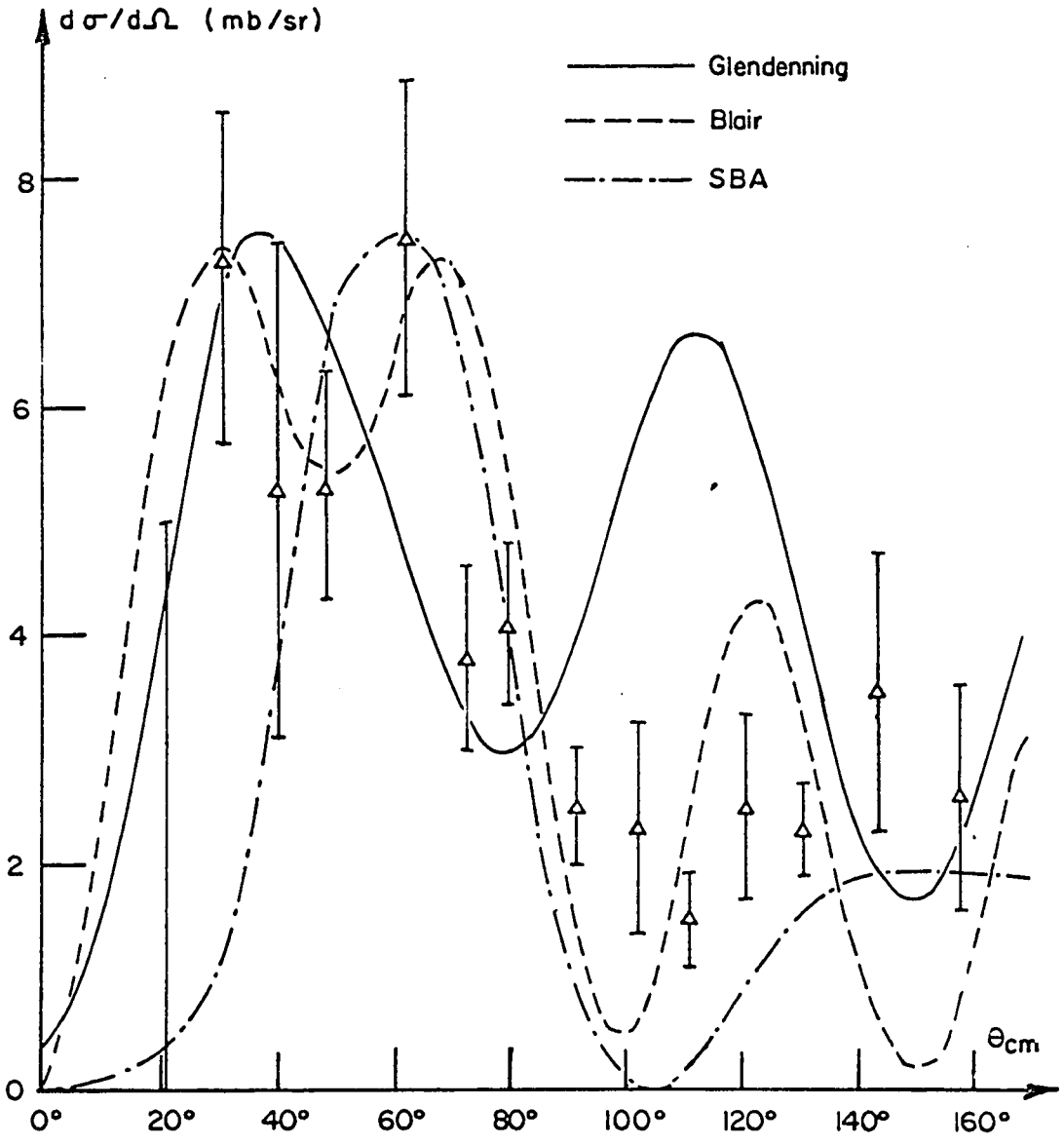
dσ/dΩ (mb/sr)
Glendenning
Blair
SBA
8
6
4
2
0
θcm
0°
20°
40°
60°
80°
100°
120°
140°
160°

collective nuclear wave function. This finding is in agreement with the generally accepted statement originally given by Glendenning[45] that the shape of the direct inelastic scattering cross sections are insensitive to the nuclear wave functions. Thus it would appear that the radial distribution of the interaction is important. In particular, the disagreement between the earlier Glendenning calculation and the present DWB result probably arises because the direct interactions were constrained to a sharp surface region in the former case. This finding is in contrast with the results of Clarke and Cross[37] who found that the shape of the anguler distribution for 14 MeV neutrons scattered by some 2+ states were fitted equally well using a DWB calculation similar to that of the present work or the simple Glendenning calculation. However Bassel et al[46] have found similar sensitivity to the radial distribution of the interaction in the case of alpha particle scattering.

From the agreement between the present DWB calculation for Ca^{40} ($Q = -3.73$ MeV), in which the direct interactions were constrained to a broad surface region (appendix A) and the recent Glendenning calculation, in which interactions were allowed throughout the nuclear volume, it would appear that the interior of the nucleus is unimportant in the direct reaction process, and most of the scattering occurs in the surface region. This is due primarily to the strong absorption which occurs in the nuclear interior.

The predictions of the plane wave Born (PWB) approximation (appendix A) and the Blair black nucleus diffraction model[15] have also been compared with the Ca^{40} data in figure 12 and table III. It is

interesting that the shape of the angular distribution curve for each of these models shows some agreement with experiment. However, little significance should be attached to this agreement since serious approximations have been made in both cases. In particular, both models use plane waves and allow adjustment of the nuclear radius to obtain the best agreement with experiment.

The values for β_3, deduced from the fitting (table III), are also interesting. The estimate based on the Blair model, which accounts for some distortion of the plane waves by removing the flux which strikes the nucleus from the beam, is in fair agreement with the DWB and electron scattering values. On the other hand, PWB model, which is based on the assumption of no distortion, gives a very poor value. The same situation has been observed in the case of inelastic proton scattering[17].

Attempts were made to fit the observed angular distribution of neutrons corresponding to the peak C of figure 9 using DWB calculations. These were based on the assumptions of collective rotational and octupole excitations of the known 3- state at 6.7 MeV and the 2+ state at 7.1 MeV respectively. The results were inconclusive due to large experimental uncertainties.

b) Energy, Yield and Angular Distribution of Gamma Rays

i) Experiment: The energies and angular distributions of gamma rays which are emitted as a result of $(n, n'\gamma)$ processes in O^{16} and Ca^{40} have been measured using a 5 in diameter by 4 in long NaI (Tl) detector. The experimental arrangement was similar to that shown in figure 1 but with the NaI detector replacing the neutron detector.

Also, much less shielding was required (4 in of lead placed immediately around the detector). The time of flight apparatus was used to distinguish between gamma rays and scattered neutrons. This technique has been used previously by Day[47] and by Deuchars and Dandy[48] to study gamma rays resulting from (n, n' γ) events which were induced by a pulsed neutron source. The basic electronic system is illustrated in the schematic diagram of figure 13. In addition to the apparatus shown, the single channel analysers and compensation circuit were used.

A typical time spectrum, obtained using a carbon target, is shown in figure 14. The flight path in this case was 88 cm and made an angle of 63 degrees with the direction of the incident neutron beam. The spectrum illustrates the discrimination which was achieved between the gamma rays (right hand peak) and the neutrons (left hand peak). By placing a window over the gamma peak with the single channel analyser of figure 13, it was possible to gate the 200 channel analyser so that the gamma ray events were recorded.

ii) Energy and Yield Measurements: Two spectra of gamma rays emitted by water under 14.1 MeV neutron bombardment are shown in figure 15. They were obtained using a water target contained in a 600 ml glass beaker (10 cm inside diameter) which was placed 20 cm from the neutron source. The gamma detector was located 50 cm from the sample at 95 degrees to the incident neutron beam. This measurement of the water gamma rays and the cascade gamma ray measurements to be described below were actually the earliest measurements performed, and tube circuits were used for the limiting preamplifiers and the TAC circuit instead of the transistorized apparatus described in chapter II and appendix C. Also, no compensation circuit was employed, and the

Figure 13: Electronics for the (n,n'γ) experiments.

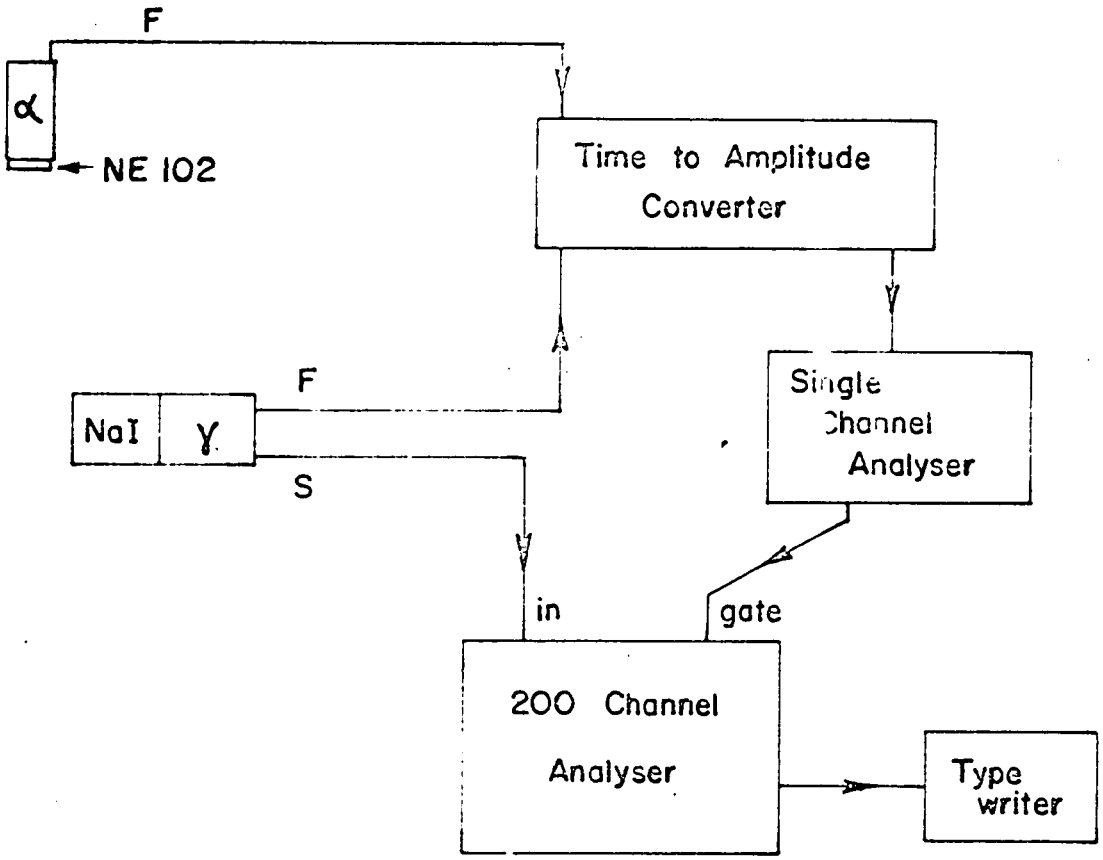
F
α
NE 102
Time to Amplitude Converter
NaI
γ
F
S
Single Channel Analyser
in
gate
200 Channel Analyser
Type writer

Figure 14: Time of flight spectrum obtained for a carbon scatterer using the 5 in diameter by 4 in long NaI detector. Time increases from right to left. 1 channel corresponds to 0.31 ns.

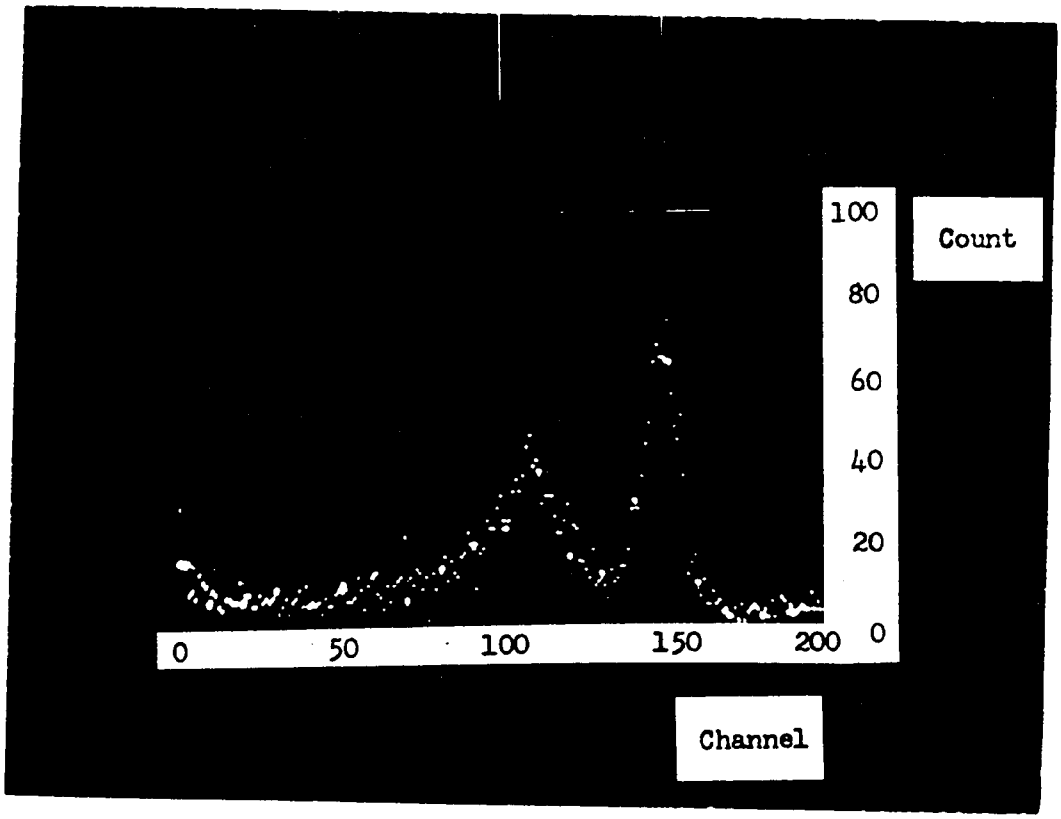
100
80
60
40
20
0
Count
0
50
100
150
200
Channel

Figure 15: Gamma ray spectra for the water target. The energies of the peaks have been obtained using the calibration sources described in the text. The level scheme is taken from reference 26).

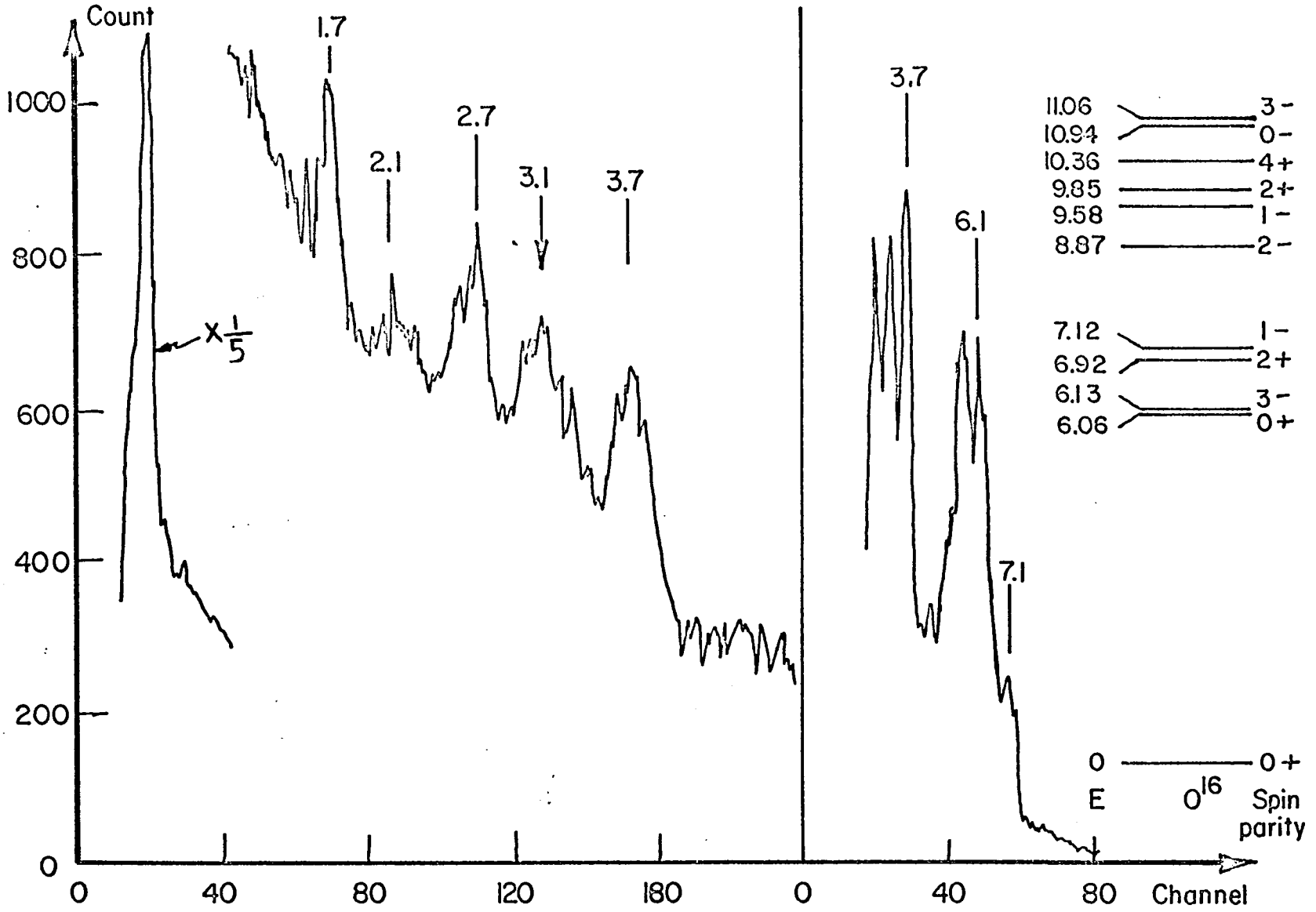
Count
1000
800
600
400
200
0
X 1/5
1.7
2.1
2.7
3.1
3.7
3.7
6.1
7.1
0
40
80
120
180
0
40
80
Channel
11.06
10.94
10.36
9.85
9.58
8.87
7.12
6.92
6.13
6.06
3 -
0 -
4 +
2 +
1 -
2 -
1 -
2 +
3 -
0 +
0
0 +
E
O16
Spin
parity

shape of the coincident neutron beam was circular in cross section with a roughly gaussian shaped profile. Two runs were performed, one with a high gain to observe the low energy part of the spectrum (left hand spectrum of figure 15) and a second with a low gain to observe the high energy part (right hand spectrum). The energy level scheme of the paper by Bromley et al[26] has been included in figure 15 for reference. The energies of the gamma rays responsible for the various peaks have been determined from a previous calibration of the detector. The following set of standard sources had been used for this calibration

Source	Energy (MeV)
Na^{22}	0.511
Cs^{137}	0.662
Co^{60}	1.17, 1.33
Thorium Oxide	2.62
RaD - Be	4.43

A linear extrapolation was used for the high energy peaks.

The prominent feature of the high energy portion of the spectrum is a 6.1 MeV peak which must correspond to decay of the 6.13 MeV 3- state since the 0+ state at 6.06 MeV cannot decay to the 0+ ground state by gamma emission. The peak just to the left of the 6.1 MeV peak corresponds to the loss of one 0.511 MeV annihilation quantum following a pair production process involving a 6.1 MeV gamma ray. The small hump still further to the left corresponds to the loss of both 0.511 MeV quanta. This triple peak response to monoenergetic

gamma rays is typical for NaI at high energies. There is also some evidence for 7.1 and 8.9 MeV gamma rays which likely correspond to ground state transitions from the 1- level at 7.12 MeV and the 2- level at 8.87 MeV respectively, although a contribution to the 7.1 MeV peak due to ground state transitions from the 6.91 MeV (2+) level is possible. The low energy spectrum indicates 1.74, 2.1 and 2.74 MeV gamma rays. These have all been identified as transitions between the O^{16} levels with the aid of a coincidence measurement to be described below. In addition there are 3.1 and 3.7 MeV gamma rays, which are due to deexcitation of the first two levels in C^{13} following the $O^{16}(n, \alpha)\ C^{13*}$ reaction, and a 0.51 MeV peak, which represents annihilation radiation from pair production processes in the target.

The relative yields for gamma rays emitted at 90 degrees to the incident neutron beam have been obtained from data similar to that of figure 15 but having all the relevant peaks in one spectrum so that normalization of two sets of data would not be required. Estimation of the contributions of individual gamma ray peaks to the spectrum was aided by knowledge of the spectrum shape for monoenergetic gamma rays obtained using the standard sources mentioned earlier. The detector efficiency as a function of energy was required for the estimation of relative yield. Since the full energy peaks were easiest to recognise in the spectrum, the photo peak or full energy peak efficiency η' was needed. This was obtained by multiplying calculated values of the total efficiency $\eta^{50)}$ by calculated values of a quantity called the photo fraction, which is the ratio between the counts in the full energy peak to the total number of counts in the spectrum for a

monoenergetic source[51]. The total efficiency and photofraction for a cylindrical detector are somewhat dependent on the source to detector distance. For this reason, adjustments were made to obtain the efficiency η' appropriate to the distance used in the present case. The resulting full energy peak efficiency for the 5 in diam. by 4 in long NaI detector is given in figure 16.

The relative yields estimated for gamma rays emitted by water at 90 degrees to the incident beam are given in table IV. The errors indicated were due mainly to the difficulty in estimating the background level beneath each peak.

The absolute yield of 6.1 MeV gamma rays following 14.1 MeV neutron bombardment of water was obtained in two ways. First, from the data which had been used to determine the relative yields, an order of magnitude estimate of 100 mb was obtained, the accuracy being seriously limited because the neutron beam shape was not well known at the time of this measurement. For this estimation, as well as the absolute yield determinations to be discussed below, the angular distribution of gamma rays was assumed to be isotropic. The effect of this assumption will be clear when the angular distribution measurements for the gamma rays have been discussed. Compared with the other uncertainties in the absolute yield determination, the error which resulted was not too serious.

A somewhat better estimate was obtained by comparing the yield of 6.1 MeV gamma rays from water with the yield of 4.43 MeV gamma rays from a carbon block measured using the same experimental geometry. By using the cross section for excitation of the 4.43 MeV 2+ state in C^{12} measured by Clarke and Cross[37] ($\bar{\sigma}(4.43) = 209 \pm 20$ mb) and by

Figure 16: Full energy peak efficiency for a 5 in diameter by 4 in long NaI detector (based on the calculated efficiency and photo fraction values of references 50, 51).

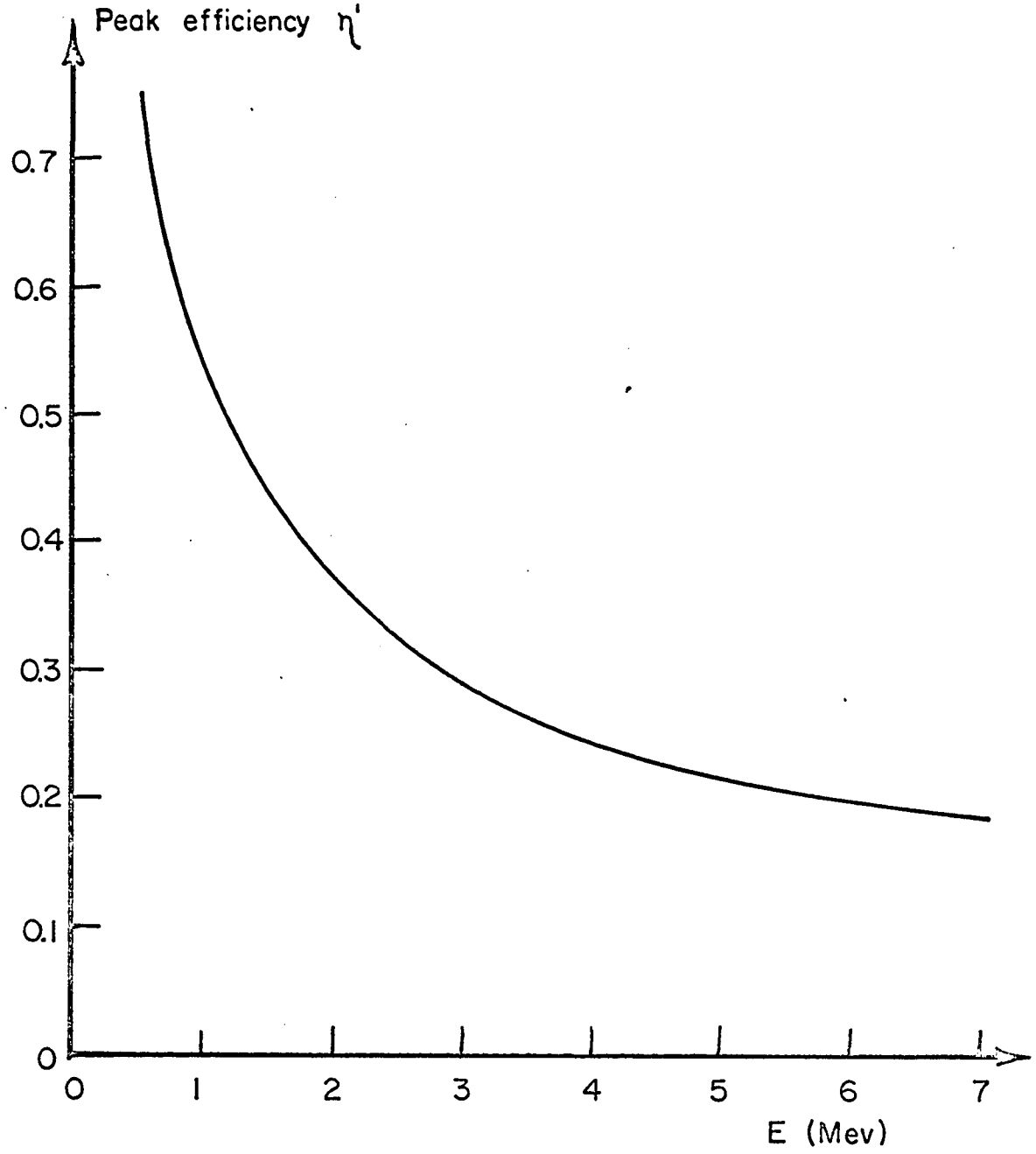
Peak efficiency η'
0.7
0.6
0.5
0.4
0.3
0.2
0.1
0
0
1
2
3
4
5
6
7
E (Mev)

TABLE IV

RELATIVE YIELD OF GAMMA RAYS FROM WATER AND CALCIUM

UNDER 14.1 MeV NEUTRON BOMBARDMENT

Target	E (MeV)	Relative Yield
Water	1.74	0.05 ± 0.03
($\theta = 90^\circ$)	2.1	0.03 ± 0.02
	2.74	0.19 ± 0.05
	3.1	0.18 ± 0.10
	3.7	0.50 ± 0.10
	6.1	1.0 (basis of normalization)
	7.1	0.39 ± 0.10
Calcium	0.8	0.48 ± 0.10
($\theta = 38^\circ$)	1.2	0.10 ± 0.03
	1.7	0.37 ± 0.10
	3.7	1.0 (basis of normalization)

calculating the number of C^{12} and O^{16} nuclei present in the targets, it was possible to obtain a value of $\bar{\sigma} = 120 \pm 40$ mb for the 6.1 MeV gamma ray yield from water.

To obtain a spectrum of the gamma rays emitted by calcium under 14.1 MeV neutron bombardment, a solid calcium metal block was used. The dimensions of the block were 4.9 cm by 14.75 cm by 14.75 cm. It was placed in the centre of the neutron beam, with a small face perpendicular to the beam direction, such that the centre of the block was 22.9 cm from the neutron source. Figure 17 shows the spectrum obtained with the gamma detector located 82.4 cm from the target at an angle of 38 degrees to the incident neutron beam. Gamma rays having energies of 3.7, 1.7, 1.2 and 0.8 MeV as well as an annihilation radiation peak at 0.5 MeV were observed. The relative intensities are given in table IV. The 3.7 MeV gamma ray peak apparently represents the ground state transition from the 3- state at 3.73 MeV. The line width for this peak suggests that only one gamma ray is contributing. Thus it would seem that the 2 + state at 3.9 MeV is not strongly excited. This observation is in accord with the good result obtained in fitting the neutron scattering data ($Q = -3.7$ MeV) when it was assumed that only the 3- state was excited.

The 0.8 and 1.7 MeV gamma rays may be due to ground state transitions from the 0.798, 0.890 and 1.64 MeV states in K^{40} following the $Ca^{40}(n,p)\ K^{40*}$ reaction. Such transitions have been observed for the case of 4 MeV neutron bombardment of calcium[33].

There were no ground state transitions observed for the level or levels near 6.7 MeV, which are excited by the neutron scattering process

Figure 17: Gamma ray spectrum for the calcium metal target. The level scheme data has been taken from references 32, 33).

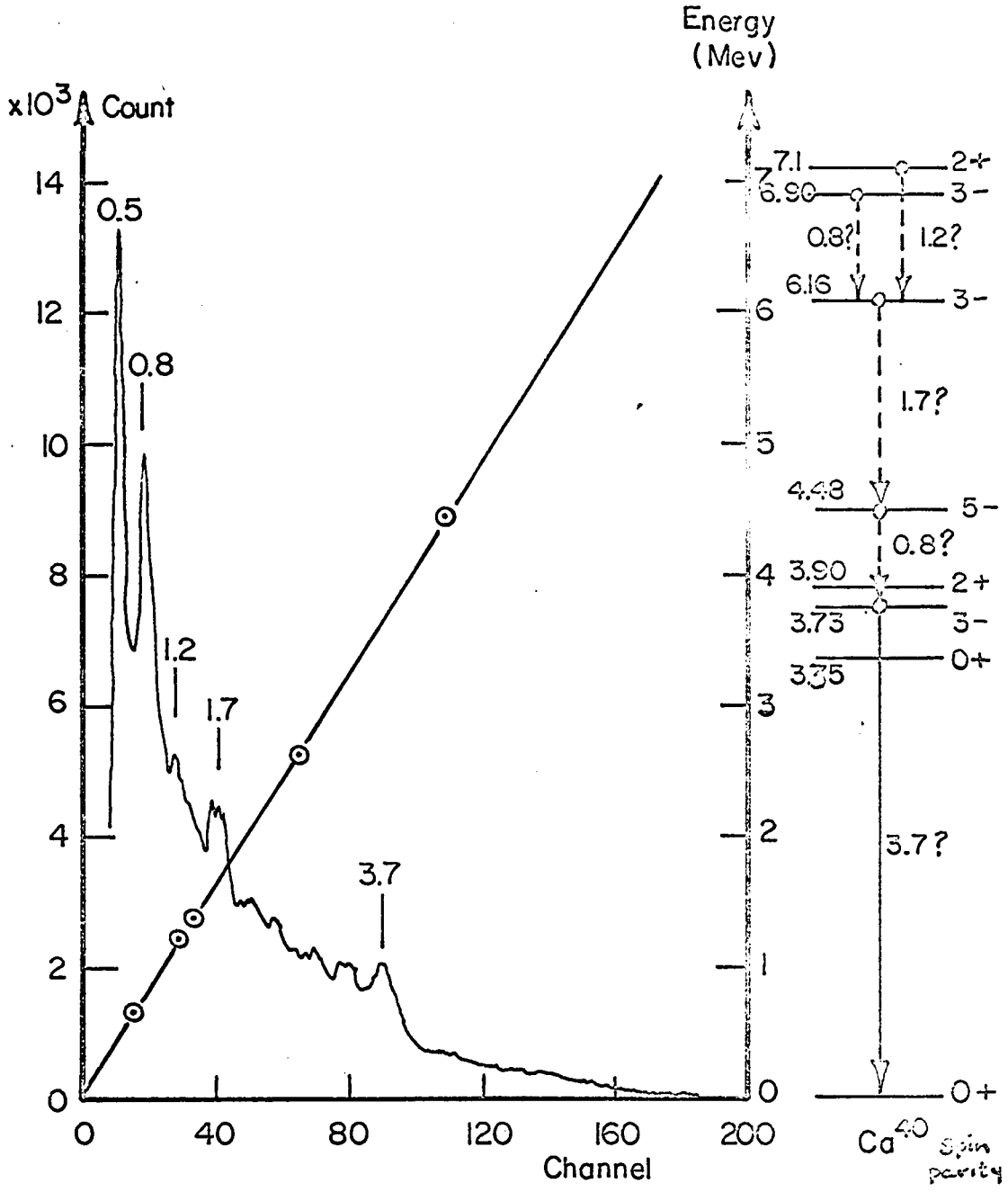
Energy
(Mev)
x10³ Count
14
12
10
8
6
4
2
0
0.5
0.8
1.2
1.7
3.7
0
40
80
120
160
200
Channel
7
6
5
4
3
2
1
0
7.1
2+
6.90
3-
0.8?
1.2?
6.16
3-
1.7?
4.48
5-
0.8?
3.90
2+
3.73
3-
3.35
0+
3.7?
0+
Ca⁴⁰
Spin
parity

(recall figure 9). Thus it is reasonable to expect that these levels may decay through cascade events which involve the 3.73 MeV state. One possible cascade is indicated on the level diagram of figure 16. However, while this cascade is consistent with the present data, it does not agree with the branching ratio observed by Rowe et al[52] who found that this state decays by a ground state transition 78% of the time and through the 3.73 MeV 3- state only 22% of the time. In any event, the true decay scheme must remain a matter of conjecture until more information is available. For example, data from coincidence measurements like those to be described later might clarify the picture.

The absolute yield of the 3.7 MeV gamma rays from calcium will be considered in the next section following discussion of the angular distribution measurements.

iii) Angular Distribution of Gamma Rays: Spectra of the gamma rays emitted at angles between zero and 156 degrees for water and calcium targets were obtained by moving the detector to appropriate positions on an arc of radius 85 cm centred on the target position. The beaker, which was used previously to contain the water sample, was replaced with a larger one (2000 ml, inside diameter 12.7 cm filled to a depth of 13.4 cm). This was placed with its centre 22.9 cm from the neutron source. In this way, the edges of the neutron beam (figure 2) defined a roughly slab-shaped scatterer subtending an angle of about 10 degrees in the scattering plane. Under these conditions the overall angular resolution was about 15 degrees. The same sample and sample position used previously for the calcium measurement were employed for the angular distribution measurement on calcium. The angular resolution in this case was also about 15 degrees.

For every gamma ray observed, the variation of intensity with angle was weak. Only in the case of the strong 6.1 MeV gamma ray from water and that of the 3.7 MeV gamma ray from calcium was it possible to see clear deviations from isotropy. The relative angular distributions for these two transitions are shown in figures 18 and 19. Corrections for attenuation of the neutron beam and the gamma radiation have been applied. The errors indicated were due to statistical uncertainties, variations in the beam profile and the sample position, as well as background subtraction and attenuation uncertainties.

The predicted angular distribution of gamma rays following an $(n,n'\gamma)$ reaction in the case of direct inelastic scattering has been calculated in the PWB approximation for the two cases using expressions given by Satchler[18]. The smooth curves of figures 18 and 19 are the result. It can be seen that the predictions agree fairly well with the gross features of the observed angular distributions even though the latter most likely contain contributions from cascade events that are not taken into account by the theory.

The yield of 3.7 MeV gamma rays from calcium relative to that of 6.1 MeV gamma rays from water was obtained by comparing the calcium and water spectra taking into account the observed angular distributions. The result was used along with the relative numbers of Ca^{40} and O^{16} nuclei present in the samples and the measured yield cross section for production of the 6.1 MeV gammas to obtain the yield cross section for production of 3.7 MeV gamma rays. The value obtained was $\sigma(3.7) = 83 \pm 40$ mb, which may be in fair agreement with the excitation cross section for the 3.73 MeV 3- state obtained from the neutron scattering

Figure 18: Angular distribution of 6.1 MeV gamma rays from water. The curve represents the PWB result.

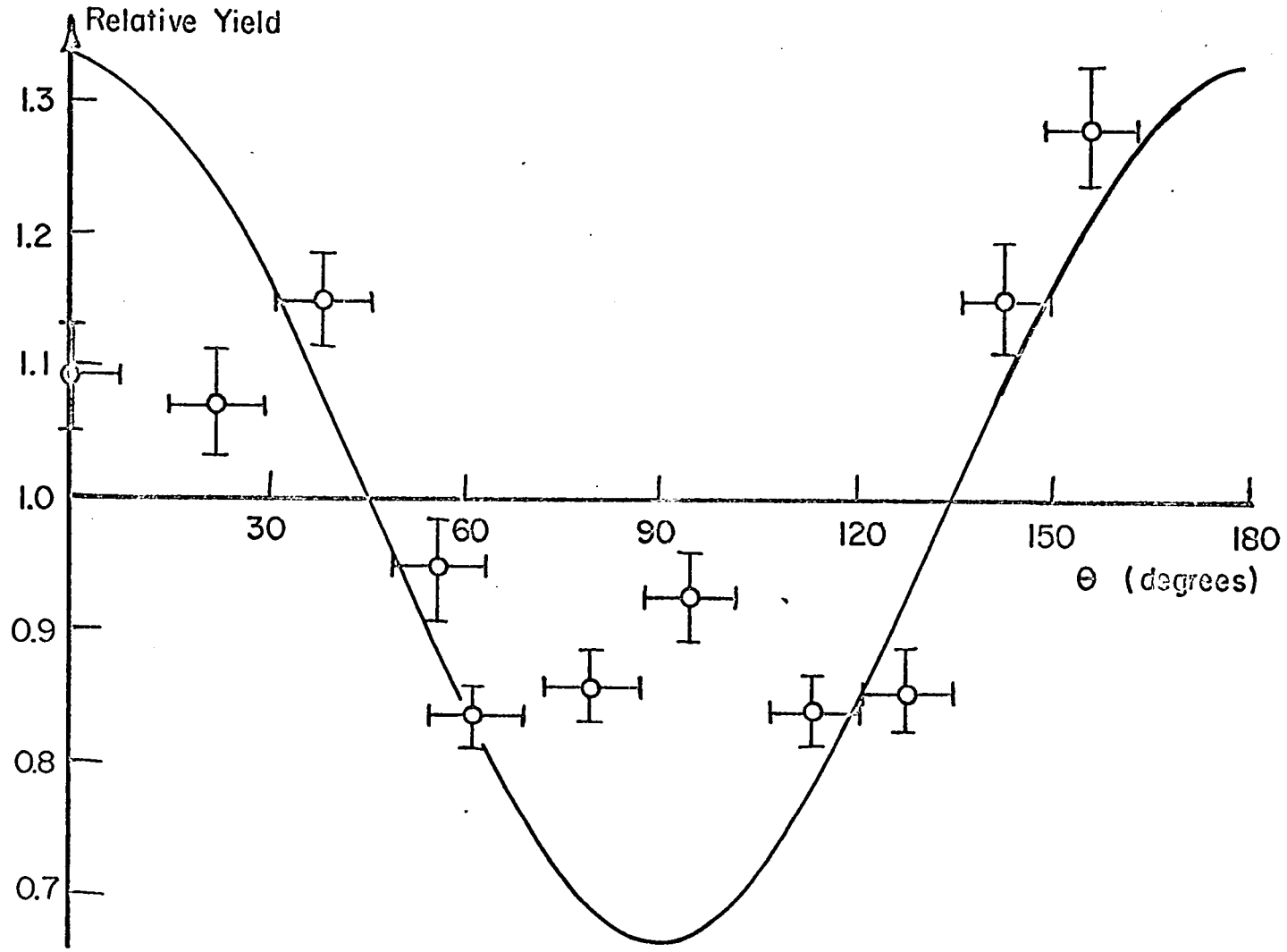
Relative Yield
1.3
1.2
1.1
1.0
0.9
0.8
0.7
30
60
90
120
150
180
Θ (degrees)

Figure 19: Angular distribution of 3.7 MeV gamma rays from calcium metal. The curve represents the PWB result.

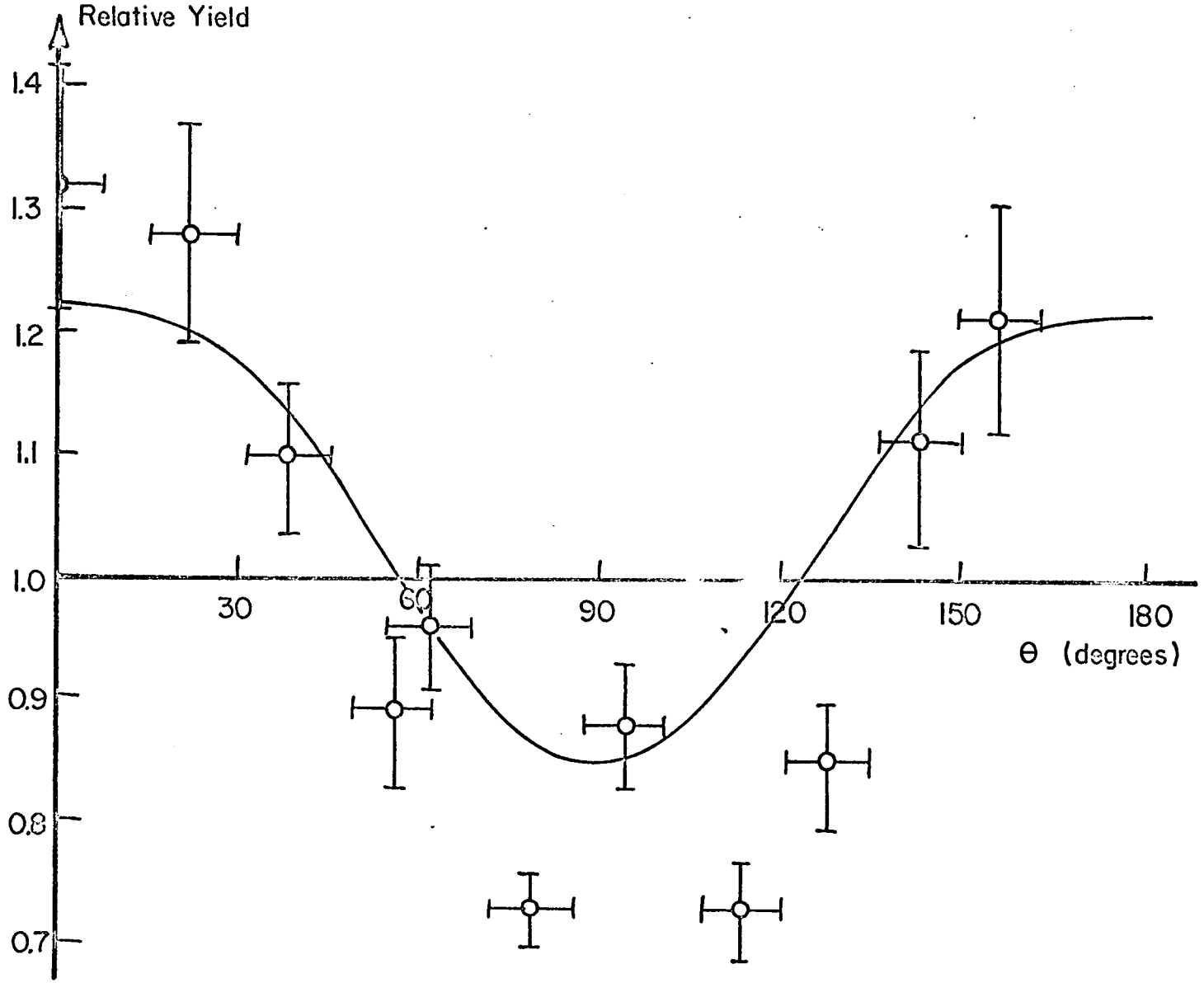
Relative Yield
1.4
1.3
1.2
1.1
1.0
0.9
0.8
0.7
30
60
90
120
150
180
θ (degrees)

experiment ($\bar{\sigma}(3-) = 43 \pm 10$ mb) if some of the lower energy gamma rays observed are cascading through this state.

c) The $O^{16}(n,n'\gamma\gamma)\ O^{16}$ Reaction

i) Experiment: In order to investigate events of the type $(n,n'\gamma\gamma)$ cascading through the 6.13 and 7.12 MeV O^{16} states, the apparatus shown in figure 20 was used. In addition to the 5 in diameter by 4 in long NaI detector, a 3 in diameter by 2 in long NaI detector was employed. A fast triple coincidence was demanded between the gamma ray and alpha detectors. Then by selecting pulses of the appropriate height from the small detector, it was possible to observe those radiations striking the large detector which were coincident in time with the detection of either a 6.1 or a 7.1 MeV gamma ray in the small detector. A 2000 ml beaker was used to contain the water target. The detectors were placed on opposite sides of the beaker with their axes on a line oriented at 90 degrees to the direction of the incident neutron beam. The front face of the large detector was located 7.1 cm from the centre of the beaker, while that of the small detector was 9.8 cm from the same point. With the detectors placed so close to the target it was not possible to use the time of flight technique to distinguish between neutron and gamma ray events. Instead it was simply used to demand a fast coincidence between pulses from the alpha detector and one of the gamma ray detectors. This was done by setting a 10 ns window over the combined neutron and gamma time peak with the single channel analyser of figure 13. Then a standard fast coincidence circuit (resolving time $2\tau = 30$ ns) was employed to demand a coincidence between pulses from the two gamma ray detectors. These two fast

Figure 20: Apparatus used in the $(n,n'\gamma\gamma)$ experiment (not to scale).

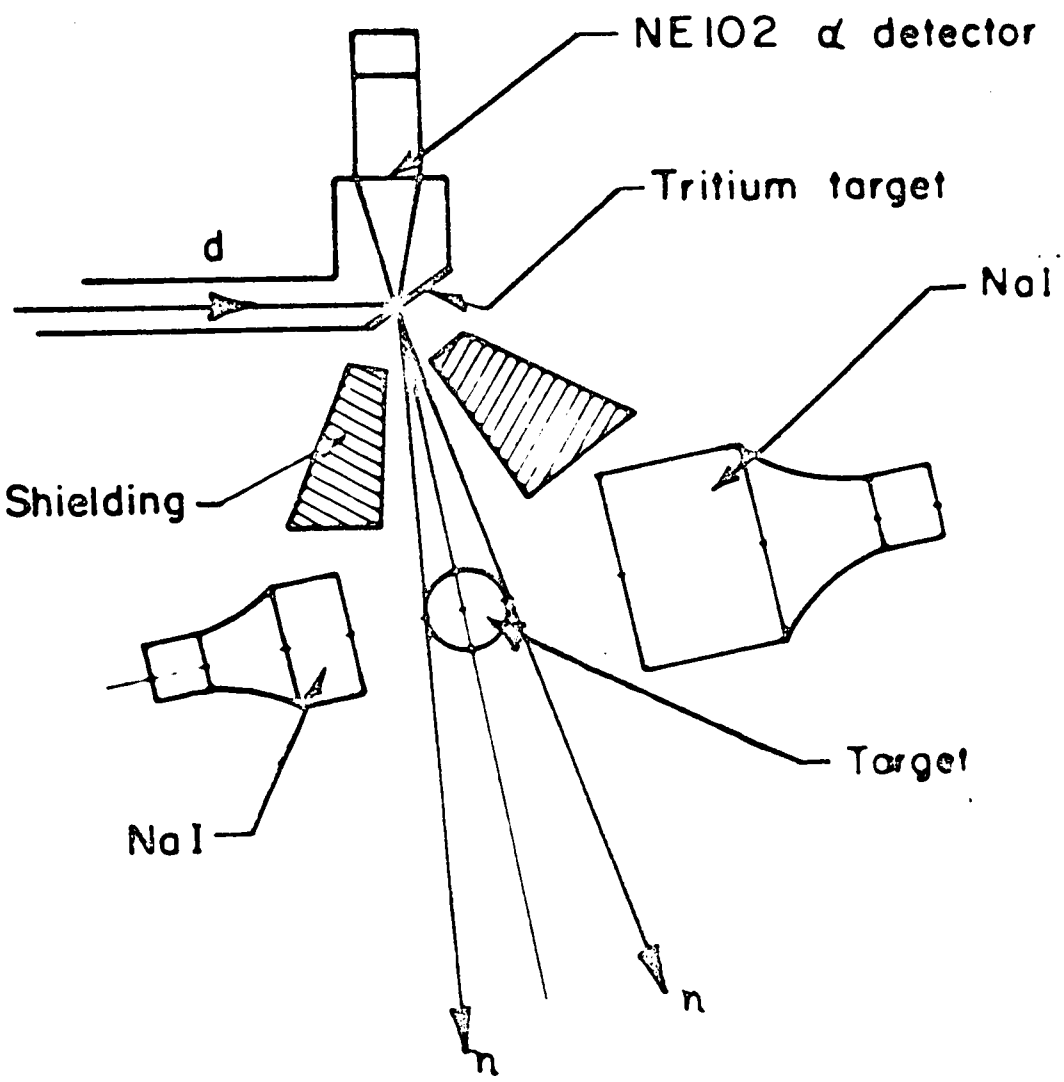
NE102 α detector
Tritium target
d
NaI
Shielding
Target
NaI
n
n

coincidence requirements were equivalent to a single triple coincidence requirement. As before, single channel analysers were used on the slow outputs of the detectors to select pulses of the desired amplitude. The outputs of all the single channel analysers and the fast coincidence circuit were combined using a slow coincidence circuit whose output controlled the multichannel analyser. The latter was fed by a linear output pulse from the large gamma ray detector.

Direct neutron bombardment of the two gamma ray detectors was inhibited by the use of shielding as indicated in figure 20, but it was not possible to prevent a scattered neutron background. The effect of this background was not serious in the case of the small detector because few of the neutrons produced pulses as large as those which resulted from detection of the high energy gamma rays. In the case of the large detector, the neutron background was important. However, since the pulse height distribution for the neutrons was a slowly varying function of energy, it was possible to see gamma ray peaks above it.

A spectrum of gamma rays from the water target observed using the 3 in diameter by 2 in long detector is shown in figure 21. The positions of a single channel analyser window, used to select either the 6.1 or the 7.1 MeV gamma ray are also shown. The dashed lines indicate the probable contributions of the individual 6.1 and 7.1 MeV gamma rays to the spectrum. These have been estimated using spectrum shapes observed for the standard sources. It can be seen that the full energy peak is smaller relative to the escape peaks than was the case for the large detector. It is to be noted that the window position used to select 6.1 MeV gamma rays allows some 7.1 MeV gamma

Figure 21: Gamma ray spectrum for water obtained with the 3 in diameter by 2 in long NaI detector. The dashed lines indicate the assumed contributions of 6.1 and 7.1 MeV gamma rays to the spectrum. The hatched areas show the two positions of the single channel analyser window which were used.

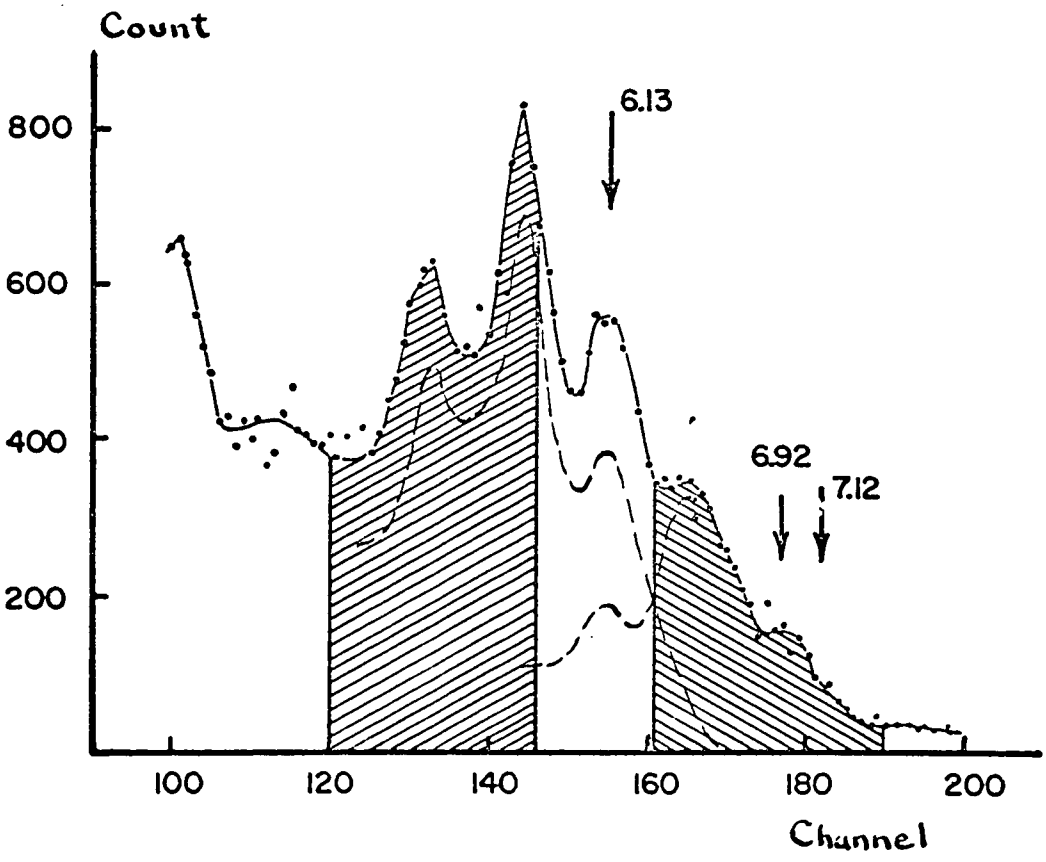
Count
800
600
400
200
6.13
6.92
7.12
100
120
140
160
180
200
Channel

ray contribution and that 6.9 MeV gamma rays from the 2+ state would not be distinguished from the 7.1 MeV gammas if they should occur.

ii) Results: The results which were obtained are shown in figure 22. It is clear that the 2.7 MeV gamma ray of the singles spectrum is in coincidence with the 6.1 MeV gamma ray (upper spectrum), while the 1.7 MeV transition is in coincidence with the 7.1 MeV gamma ray (lower spectrum). There is a small peak at 1.8 MeV in the upper spectrum. This is no doubt due to the inclusion of a portion of the 7.1 MeV spectrum in the window used to select the 6.1 MeV events. In addition there is a 2.1 MeV peak visible in both spectra. In the upper spectrum, part of this peak is due to the escape of single annihilation quanta following pair production processes involving the 2.7 MeV gamma ray. However, this does not completely account for the magnitude of the peak, and it would appear that there is a weak 2.1 MeV gamma ray cascading down through the 8.87 MeV 2- state as shown in the level scheme. This cascade probably originates at the 3^+ state at 11.06 MeV as shown rather than the 10.94 MeV 2- level since the measured branching ratio for the latter state[26] would require that a very strong 3.8 MeV gamma ray also be seen and there is no evidence for such a transition in the present data.

Using the data of figure 21, the branching ratio of the 8.87 MeV state has been estimated to be 0.14 ± 0.15 going to the 1- (and/or the 2+) state at 7.12 MeV relative to unity going to the 6.13 MeV 3- state. This result is in reasonable agreement with the values of 0.189 observed by Bromley et al[26] and 0.11 observed by Wilkinson et al[53].

In addition, the data of the coincidence measurement coupled with that of the single detector gamma ray measurements leads to the decay

Figure 22: Spectra of the gamma rays which were in coincidence with 6.1 MeV gammas (upper spectrum) and with 7.1 MeV gammas (lower spectrum) for a water target.

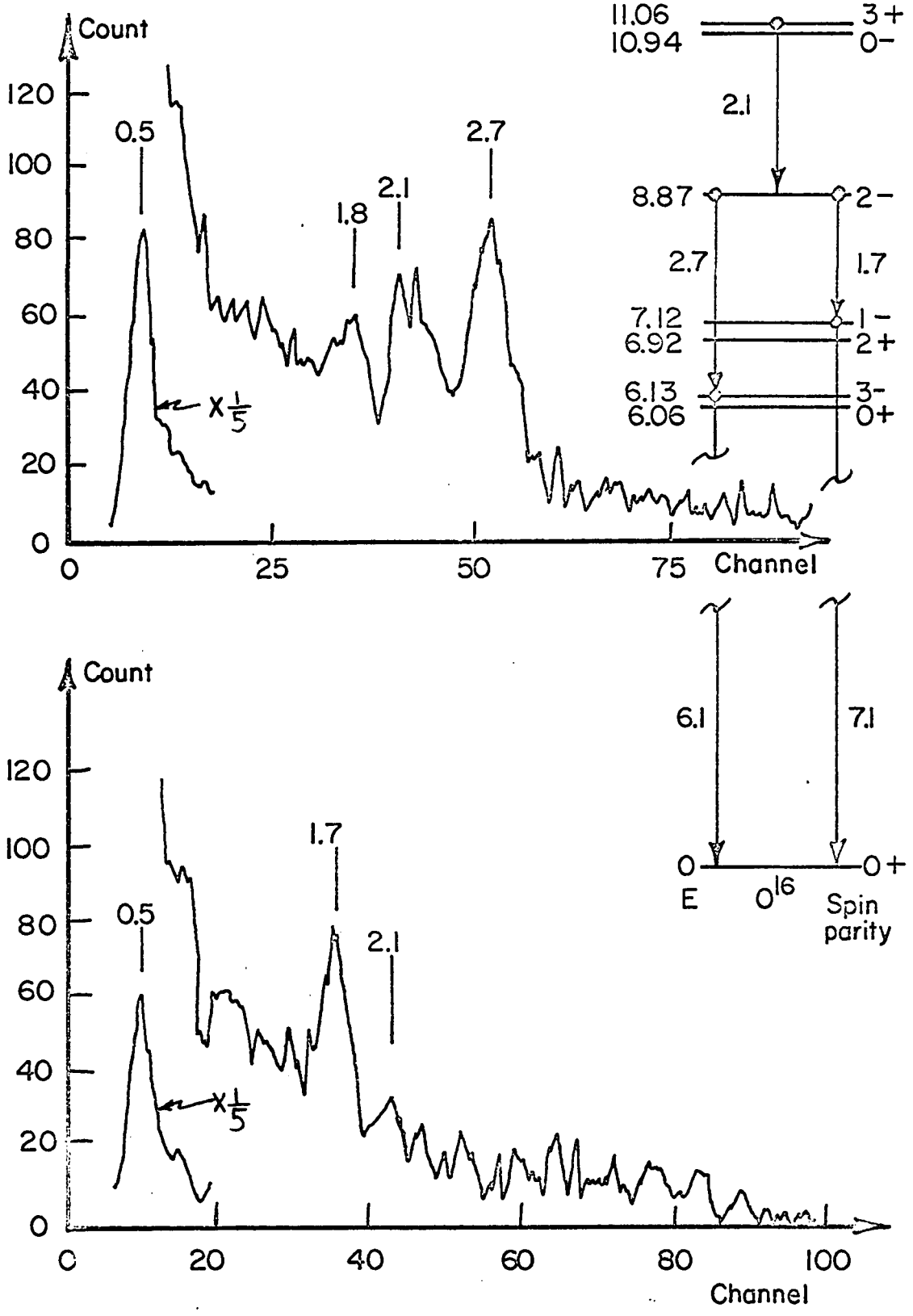
Count
120
100
80
60
40
20
0
0.5
1.8
2.1
2.7
X 1/5
0
25
50
75
Channel
11.06
10.94
3+
0−
2.1
8.87
2−
2.7
1.7
7.12
6.92
1−
2+
6.13
6.06
3−
0+
Count
120
100
80
60
40
20
0
0.5
1.7
2.1
X 1/5
0
20
40
60
80
100
Channel
6.1
7.1
0
0+
E
O16
Spin parity

scheme indicated on the level diagram of figure 22. Using this decay scheme and the relative yield data of table IV, the relative cross sections for excitation of the various states in O^{16} have been calculated. These are compared with the corresponding values obtained from the neutron scattering data of the present work and that of Perey[54] in table V. The agreement is good with the exception of the high value obtained from the neutron data of the present work for excitation of the 7.12 MeV 1- state. This discrepancy is probably due to errors in resolving the 6.1 and 7 MeV peaks of the neutron data. Perey's result for this ratio should be more accurate since he used a higher bias and a smaller detector for the neutrons and was therefore able to obtain a better separation of these peaks.

On the basis of the data of table IV and the absolute yield of 6.1 MeV gamma rays, the absolute cross section for excitation of the 6.13 MeV 3- state in O^{16} was estimated to be 95 ± 40 mb. This is in reasonable agreement with the corresponding value obtained from the neutron scattering data of 76 ± 15 mb.

TABLE V

RELATIVE CROSS SECTIONS FOR (n, n') REACTIONS IN O^{16}

State	Neutron Scattering Data (present work)	(Perey[54])	Gamma Ray Data
ground (0+)	11.7	10.5	
6.13 MeV (3-)	1	1	1
7.12 MeV (1-)	0.67	0.41	0.43 ± 0.15
8.87 MeV (2-)	0.23		0.27 ± 0.10
11.06 MeV (3+)	0.03		0.04 ± 0.03

CHAPTER III

CONCLUSIONS

The $(n,n'\gamma)$ reaction has been studied in some detail for O^{16} and Ca^{40} in order to investigate the occurrence and nature of collective octupole vibrations in these nuclei.

The excitation process was examined by measuring differential cross sections for the inelastically scattered neutron groups. Significantly, the strongest excitation occurred at the energy corresponding to the lowest 3- state in each case. This is a good indication that there are collective correlations in the nucleon motions that are responsible for these 3- states[6,7].

The optical model was used to fit the elastic scattering cross sections. Good agreement was obtained, and the optical model parameters which resulted were similar to those found by previous workers.

The optical parameters were employed in a DWB calculation to predict the direct inelastic scattering cross sections for the lowest 3- states in O^{16} and Ca^{40}. The latter states were represented by octupole vibrations for the DWB calculations. For the O^{16} state a compound nucleus contribution, estimated using the statistical model, was added to the calculated cross section for direct inelastic scattering. In the case of Ca^{40}, the shape of the predicted cross section was in very good agreement with experiment. When the magnitude of the predicted cross section was adjusted to fit experiment,

a value of the collective deformation parameter β_3 was predicted which agrees well with values found from electron scattering data[32, 41,42]. Quite recently, similar agreement has been found by Yagi et al for the case of inelastic proton scattering by Ca^{40} (Q = -3.7 MeV) at 55 MeV when a DWB calculation based on an octupole excitation was assumed[55]. The fact that the DWB model works so well for these two cases is a striking justification of the DWB method because different projectiles were used and the bombarding energies differed by a factor of 4. Another interesting observation which can be made concerning these two sets of data is that a marked similarity exists between the overall appearance of the scattered neutron and proton spectra. In particular, the strongest scattering observed in the proton experiment was due to a state at an excitation of 3.7 MeV, and this was followed by weaker scattering due to a state at 6.9 MeV. These results are good evidence that the direct interaction mechanism is dominating the scattering of nucleons by Ca^{40} in this energy range. If the compound nucleus process was important at 14 MeV, there would not be such a strong correlation between the spectra.

The shape of the predicted scattering cross section for O^{16} (Q = -6.13 MeV) was only in rough agreement with experiment. It is possible that errors in resolving the 6.1 and 7 MeV peaks of the time spectrum are responsible. In the region of 120 degrees the observed cross section for exciting the 7 MeV state goes through a sharp maximum to become comparable in magnitude with the 6.1 MeV cross section. Thus large errors in the 6.1 MeV data could have been made rather easily. The reason for considering such a possibility is that an

overestimate of the magnitude of the 7 MeV peak could be the reason for the bad agreement between the 6.1 MeV cross section and the DWB prediction in the 120 degree region. Such an overestimate would have contributed to the observed discrepancy between the relative cross sections observed using neutrons and gamma rays (table V).

A second possibility is that deficiencies in the theory may be responsible for the poor fit. No spin-orbit term was included in the interaction potential for the calculation, and the imaginary part of the optical potential was not allowed to become deformed. These factors would affect the result but probably not very much. Satchler et al[56] were unable to achieve a good fit to the cross section for 19 MeV proton scattering by O^{16} ($Q = -6.1$ MeV) when they allowed the imaginary part of the potential to become deformed along with the real part and the shapes of DWB scattering cross sections are generally found to be insensitive to the spin-orbit part of the interaction[20]. A more likely possibility is that the DWB method is just not good enough in the case of such a light nucleus, especially when the collective enhancement is very strong. A recent comparison by Stamp and Rook[57] has indicated that the DWB model does not give the same results as the more accurate coupled equation method when used for a light nucleus if there is strong deformation. In fact, it is not at all certain that the optical model should be used for a nucleus having only 16 nucleons even though the elastic data are fairly well fitted. In particular, it is a weak assumption to rely on the radial form factor defined by the smooth optical model potential to produce the direct interaction scattering.

It is not possible to decide between these possibilities on the basis of the present experiment. One can only conclude that the DWB method provides at least a rough fit for O^{16} ($Q \simeq -6.1$ MeV) and hope that a more precise experiment can be performed in the future which will make it possible to determine whether theory or experiment is at fault. A time resolution of about 1.5 ns should be obtainable with a system of the size used in the present work if the electronic contributions to the time spread were eliminated or at least greatly reduced. The 6.1 and 7 MeV time peaks observed with such a system would be completely resolved.

Turning now to the time spectrum of neutrons scattered by Ca^{40}, the observed peak which corresponds to an excitation of 6.7 MeV is not understood. Attempts to fit the data using DWB calculations were inconclusive. In considering the significance of the cross sections deduced from these peaks it should be born in mind that there may be a contribution to the observed scattering due to air in the path of the coincidence beam. Such an effect would be most important at forward and backward scattering angles where the detector subtends a large region of the coincidence beam. Thus it could have contributed to the large peak observed in the cross section at backward angles. This effect was not observed in the background runs possibly because these runs were short, but it would appear that most of the observed scattering is due to the Ca^{40}.

An interesting point concerning the Ca^{40} inelastic scattering ($Q \simeq -3.7$ MeV) is that the Blair model provided a reasonably good fit to the angular distribution and predicted a value of β_3 in fair

agreement with that found in the DWB calculation. This is an encouraging result because the nature of the reaction process is easy to visualise in the Blair model. In particular, this agreement emphasizes the diffraction-like nature of the direct interaction scattering process for neutrons.

The energies and yields have been measured for the gamma rays which are emitted when the excited states of O^{16} and Ca^{40} decay. For O^{16}, a decay scheme was obtained with the aid of an auxilliary coincidence experiment which permitted the observation of cascade gamma ray events. This decay scheme led to values for the excitation cross sections which were in agreement with the neutron scattering cross sections. A value was also obtained for the branching ratio of the 8.87 MeV 2- state in O^{16}. It is in agreement with previous measurements for this quantity.

No coincidence experiment was performed to observe gamma ray cascade events in the case of Ca^{40}, and the decay scheme for this nucleus is uncertain. However, one feature of the decay scheme for Ca^{40} which was clear is that the ground state transitions for states higher than the 3- level exist only weakly, if at all. Except for the 1- state at 7.12 MeV, the same situation holds for O^{16}. This result is in accord with the assumption of collective vibrations for the 3- states, if it is assumed that higher states are formed on top of the vibrational mode.

Angular distributions were measured for the ground state transition gamma rays from the lowest 3- states in O^{16} and Ca^{40}. The deviations from isotropy were not strong and the observed distributions were fairly well fitted using a PWB calculation. It would be

interesting to see if a more accurate theory would give a good result, because it has been suggested[20] that the gamma ray distribution is sensitive to the nuclear model used to describe the excited states. In any event, the gamma ray certainly has the chance to carry more information about the nuclear state than does the scattered neutron. The latter is only aware of the nucleus for an instant when the state is being formed, while the very existence of the gamma ray is a result of the nuclear motions. For this reason it will probably prove fruitful to pursue the gamma ray measurements further. For example, the decay scheme for Ca^{40} could probably be sorted out by using a coincidence experiment to see which gamma rays are cascading through the lowest 3- state. Then, it might be possible to observe the angular correlation of gamma rays with the scattered neutrons, although the counting rate for such a measurement would be very low.

Another useful extension of the present work would be to study the lowest 3- state in Pb^{208} using 14 MeV neutrons. Then, provided a reasonably consistent picture of octupole excitation resulted for the closed shell nuclei, a search could be made for evidence of octupole vibrations in nuclei near the closed shells. Unfortunately, the energy resolution of the neutron experiment is not good, and it would be difficult to study the excitation of nuclei having complex spectra. For such nuclei the gamma ray experiments would probably be most useful.

APPENDIX A

BORN APPROXIMATION THEORY FOR INELASTIC SCATTERING

a) General Formalism; Integro-differential Form of the Schroedinger Equation

Consider a scattering system consisting of a projectile a and a nucleus X, which has internal motions that can be described in terms of the internal coordinates ξ. Let $\vec{r}$ be the vector joining the centres of mass of a and X. Then, ignoring centre of mass motion, the Hamiltonian for the whole system can be written

$$H(\vec{r},\xi) = K(\vec{r}) + H_I(\xi) + V(\vec{r},\xi) \qquad (A1)$$

where $K(\vec{r})$ is the kinetic energy of relative motion, $H_I(\xi)$ is the Hamiltonian for the internal motion of X, and $V(\vec{r},\xi)$ is the interaction between a and X. The corresponding time independent Schroedinger equation for the system is

$$H(\vec{r},\xi)\,\Psi(\vec{r},\xi) = E\,\Psi(\vec{r},\xi)\,. \qquad (A2)$$

Now let the eigenvalues and eigenfunctions for the internal motion of X be ϵ_n and ϕ_n respectively.

$$H_I(\xi)\,\phi_n(\xi) = \epsilon_n \phi_n(\xi)\,. \qquad (A3)$$

Then the wave functions $\Psi(\vec{r},\xi)$ can be expanded in terms of the ϕ_n and ψ_n which are assumed to be complete in ξ and r respectively.

$$\Psi(\vec{r},\xi) = \sum_n \psi_n(\vec{r})\,\phi_n(\xi) \tag{A4}$$

where n refers to the scattering channel in which the nuclear state designated by n in equation (A3) is excited and $n = 0$ refers to the incident or elastic scattering channel. Using relations (A1) and (A4), equation (A2) becomes

$$\left\{K(\vec{r}) + H_I(\xi) + V(\vec{r},\xi)\right\} \sum_n \psi_n(\vec{r})\,\phi_n(\xi)$$

$$= E \sum_n \psi_n(\vec{r})\,\phi_n(\xi) \,. \tag{A5}$$

Multiply by ϕ_m^* and integrate over the coordinates ξ.

$$(K + \epsilon_m)\psi_m + \sum_n \int d\xi\, \phi_m^* V \phi_n \psi_n = E\psi_m$$

or

$$-\left\{K(\vec{r}) - (E - \epsilon_m)\right\}\psi_m(\vec{r}) = \sum_n V_{mn}(\vec{r})\,\psi_n(\vec{r}) \tag{A6}$$

where $E - \epsilon_m$ is just the energy of the relative motion and

$$V_{mn}(\vec{r}) = \int d\xi\, \phi_m^*(\xi)\, V(\vec{r},\xi)\, \phi_n(\xi) \,. \tag{A7}$$

Equation (A6) represents a set of coupled equations for the wave functions $\psi_k(\vec{r})$ of the relative motion in terms of the set $\phi_k(\xi)$, which describe the states of the scattering nucleus, and the potential $V(\vec{r},\xi)$. Writing it out in full and rearranging slightly gives

$$-\{K-(E-\epsilon_0)+V_{00}\}\psi_0 = 0 \quad + V_{01}\psi_1 + \cdots$$

$$-\{K-(E-\epsilon_1)+V_{11}\}\psi_1 = V_{10}\psi_0 + 0 + \cdots$$

$$\vdots \qquad \vdots \qquad \vdots \qquad \vdots \qquad \text{(A8)}$$

The boundary conditions for this set in the case of a beam of incident particles travelling in the direction of $\vec{k}$ are

$$\psi_0 \xrightarrow[r\to\infty]{} e^{i\vec{k}_0\cdot\vec{r}} + \left(\frac{M_0}{2\pi\hbar^2}\right)\frac{e^{ik_0 r}}{r}A_0(\theta) \qquad \text{(A9)}$$

and

$$\psi_{m\neq 0} \xrightarrow[r\to\infty]{} \left(\frac{M_m}{2\pi\hbar^2}\right)\frac{e^{ik_m r}}{r}A_m(\theta) \qquad \text{(A10)}$$

where $k_m = \frac{2\mathcal{M}_m}{\hbar^2}(E-\epsilon_m)$, $\mathcal{M}_m$ is the reduced mass in channel m, and $A_m(\theta)$ is the transition amplitude for the channel m. With this definition for $A_m(\theta)$ the scattering cross section is

$$\left(\frac{d\sigma}{d\Omega}\right)_m = \frac{M_0 M_m}{(2\pi\hbar^2)^2}\frac{k_m}{k_0}\left|A_m(\theta)\right|^2 . \qquad \text{(A11)}$$

Thus, the wave function ψ_0 is asymptotically like the sum of an incident plane wave plus an outgoing spherical wave whose amplitude is a function of θ. The functions $\psi_{m\neq 0}$ are similar but have no incoming plane wave.

Equation (A6) or the equivalent set (A8) are general except for the lack of antisymmetrization. That is, the total wave function

$\Psi(\vec{r},\xi)$, should be made antisymmetric with respect to exchange of identical particles in the system. In general this has the effect of allowing the introduction of other processes besides scattering and this effect can be accounted for sufficiently well by imaginary terms in the potential $V(\vec{r},\xi)$, which will be necessary in any event to take care of compound nucleus formation. Even neglecting the antisymmetrization, complete solutions for (A6) or (A8) would be prohibitivly complicated and approximations are usually introduced to simplify the problem. Three such approximations will be described below.

In many cases of practical interest some of the scattering amplitudes $A_{m\neq 0}(\Theta)$ are so small that the corresponding wave functions ψ_m can be neglected. For example, if the inelastic scattering excites only one state appreciably, say the one labelled k, then all the ψ_m except ψ_0 and ψ_k can be set equal to zero in (A8) yielding a pair of coupled equations.

$$\begin{aligned} -\{K-(E-\epsilon_o)+V_{oo}\}\psi_0 &= V_{ok}\psi_k \\ -\{K-(E-\epsilon_k)+V_{kk}\}\psi_k &= V_{ko}\psi_0 . \end{aligned} \tag{A12}$$

This approach is called the coupled equation (CE) approximation. It can be used, at least in principle, so long as the number of terms is finite.

A further simplification is possible if the state k is not too strongly excited in which case $V_{0k}\psi_k$ can be neglected relative to $V_{00}\psi_0$ in the upper equation of (A12). This results in a pair of uncoupled equations.

$$\left\{K - (E-\epsilon_o) + V_{oo}\right\}\psi_o = 0 \qquad \text{(A13)}$$

and

$$-\left\{K - (E-\epsilon_k) + V_{kk}\right\}\psi_k = V_{ko}\,\psi_o . \qquad \text{(A14)}$$

Now equation (A13) is just the optical model problem which can be solved in terms of the optical potential V_{oo} to yield ψ_o, a plane wave highly distorted by the elastic scattering (recall the boundary conditions (A9). In practice V_{oo} is usually determined by comparing elastic scattering cross sections, based on the solutions of (A13) found using various potentials, with experiment. This leads to a definition of V_{oo} in terms of a set of optical parameters which are found to vary slowly and smoothly with energy[9]. The solution ψ_o can be used in (A14) to solve for ψ_k, provided the potentials V_{kk} and V_{ko} are known. This is the distorted wave Born (DWB) approximation.

A more drastic approximation, which can be used if the elastic scattering itself is weak, is the plane wave Born (PWB) approximation. This is obtained by setting V_{oo} and V_{kk} equal to zero in (A13) and (A14). The solution of (A13) is then a plane wave $e^{i\vec{k}_o\cdot\vec{r}}$ and (A14) becomes

$$-\left\{K - (E-\epsilon_k)\right\}\psi_k = V_{ko}\, e^{i\vec{k}_o\cdot\vec{r}} . \qquad \text{(A15)}$$

In the case of scattering of MeV nucleons by nuclei the PWB approximation is completely unjustified because the distortion of the incident and emergent waves caused by the nuclear potential is quite serious. Its only usefulness lies in the fact that a closed form result can be

obtained which shows the essential features of the more complicated CE and DWB solutions.

In section b following, the method for solving the DWB problem is outlined and the form of the DWB cross section is obtained for the case of excitation of collective vibrational levels by inelastic scattering. In section c the complete PWB solution is given for the same case. No discussion of the CE solution is included as it was not required for the present work but the interested reader will find the articles by Chase et al[10] and Buck[11] give very good descriptions of the method.

b) The DWB Solution

i) General Form: The problem is to solve the equation (A14) for ψ_k subject to the boundary condition (A10). This can be accomplished using the Green's function method[58]. First the right hand side of (A14) is set equal to zero to yield a homogeneous equation having the same form as the optical model problem (A13). This new optical problem can be solved in terms of the potential V_{kk}, which is the optical potential for elastic scattering by the nucleus in the excited state k, to yield $\tilde{\psi}_k$. To do this the potential V_{kk} must be known. It cannot be obtained from experiment but the potential for elastic scattering of projectiles having energy $(K - \epsilon_k)$ is probably a good substitute and since optical potentials change only slowly with energy the potential V_{00} is often used for V_{kk}. The Green's function for the equation (A14) can be written in terms of the function $\tilde{\psi}_k$. Then the expression for $\psi_k(\vec{r})$ is written according to the Green's function

method,

$$\psi_k(\vec{r}) = \frac{M_k}{2\pi\hbar^2} \frac{e^{ik_k r}}{r} \times \int d\vec{r}' \bar{\psi}_k^*(\vec{r}') V_{k_0}(\vec{r}') \psi_0(\vec{r}') . \quad (A16)$$

Comparing this with the boundary condition (A9), we see that the scattering amplitude for excitation of the state k is

$$A_k(\theta) = \int d\vec{r}' \bar{\psi}_k^*(\vec{r}') V_{k_0}(\vec{r}') \psi_0(\vec{r}') . \quad (A17)$$

If this expression is substituted in (A11) the general DWB cross section for inelastic scattering results. To obtain the $A_k(\theta)$ for particular cases, it is necessary to assume some form for V_{k0}. This will be done for a case of collective excitation below.

ii) Excitation of Collective Vibrational States: In order to treat collective excitations it is convenient to make the nuclear radius a function of angle by replacing the radius parameter R of the optical model (see Chapter II for definitions of the optical parameters) by *

$$R(\Omega) = R\left[1 + \sum_{\lambda\mu} \alpha_{\lambda\mu}^* Y_{\lambda\mu}^*(\Omega)\right] \quad (A18)$$

where $\alpha_{\lambda\mu}^*$ is an expansion coefficient which may depend on time, and $Y_{\lambda\mu}^*(\Omega)$ is a spherical harmonic. Now consider the change in the real part of the optical model potential which is given by V f(r) before

*For collective model theory see Bohr and Mottelson[59] and Buck[11]. The formalism presented here is the same as that used by Buck[11].

and V f(r, R(Ω)) after the substitution (A18) where V is the well depth parameter (Chapter II). (It is customary to ignore the change in the imaginary part of the optical potential since only a first order expression will be found for the interaction potential V_{k0}.) The distorted potential V f(r, R(Ω)) can be expanded using a Taylor expansion for small α^*.

$$Vf(r, R(\Omega)) = Vf(r) + VR \sum_{\lambda\mu} \alpha^*_{\lambda\mu} Y^*_{\lambda\mu}(\Omega) \frac{\partial f(r)}{\partial r} + \cdots \quad \text{(A19)}$$

The first term is the undistorted real part of the optical potential. The second term is the first order expression for that part of the potential $V(\vec{r}, \xi)$ of equation (A7) which results in the inelastic scattering transitions that excite collective levels. In the case of vibrational levels in even-even nuclei it is convenient to think of $\alpha^*_{\lambda\mu}$ as an operator which creates one phonon vibrations of the type $\lambda\mu$ about a spherical equilibrium shape. Its matrix element between states having zero and one phonon is[11]

$$\langle 1 | \alpha^*_{\lambda\mu} | 0 \rangle = [\hbar\omega / 2C_\lambda]^{1/2} \quad \text{(A20)}$$

where $\hbar\omega$ is the phonon energy, $|n\rangle$ is the wave function for an n phonon state, and C_λ is the surface potential energy parameter of the collective model.

In the case of a nucleus having a permanent ground state deformation $\sum_\mu \alpha_{\lambda\mu}$ is replaced by β_λ, the collective model deformation parameter. In analogy to this permanent deformation parameter an

effective (root mean square) deformation parameter can be defined for the vibrational excitations[11].

$$\beta_\lambda^2 = \langle 0 | \sum_\mu |\alpha_{\lambda\mu}|^2 | 0 \rangle$$
$$= (2\lambda+1)\ \hbar\omega / 2C_\lambda . \qquad \text{(A21)}$$

Thus the potential V_{k0} of equation (A17) in the case of collective excitation of a one phonon vibrational state, characterized by the angular momentum quantum number λ, is found by substituting $V f(r,R(\Omega))$ for $V(\vec{r},\xi)$ in equation (A7) and noting that there is no contribution due to the first term of (A19).

$$V_{k0}(r') = \int d\xi\ \varphi_k^*(\xi)\, V R \times \sum_\mu \alpha_{\lambda\mu}^*\, Y_{\lambda\mu}^*(\vec{r}')\, \frac{\partial f(r')}{\partial r'}\, \varphi_0(\xi) \qquad \text{(A22)}$$

which reduces, through the use of (A20) to

$$V_{k0}(r') = \sum_\mu V R\, Y_{\lambda\mu}^*(\vec{r}')\, \frac{\partial f(r')}{\partial r'} \left[\frac{\hbar\omega}{2C_\lambda}\right]^{1/2} . \qquad \text{(A23)}$$

Thus the scattering amplitude (A17) becomes using (A21)

$$A_k(\theta) = VR\beta_\lambda / (2\lambda+1)^{1/2} \times \sum_\mu \int dr'\, \bar{\psi}_k^*(\vec{r}')\, Y_{\lambda\mu}^*(\vec{r}')\, \frac{\partial f(r')}{\partial r'}\, \psi_0(\vec{r}') , \qquad \text{(A24)}$$

and the corresponding DWB cross section for excitation of a one phonon vibrational state is obtained by putting this expression for $A_k(\theta)$ in

equation (A11).

It should be noted that the shape of the DWB cross section is determined by optical potentials V_{00} and V_{kk} and by the multipolarity of the transition through the factor $Y^*_{\lambda\mu}$ in (A24). The magnitude of the cross section depends on $(VR\beta_\lambda)^2$ and can therefore be adjusted to fit experiment by varying β_λ.

c) The PWB Solution; Excitation of Vibrational States in the Limit of a Zero Range Surface Interaction

Using the Green's function method in the same way as for the DWB case, the PWB expression (A15) leads to a scattering amplitude similar to that given by (A17) but with plane waves replacing the optical wave functions.

$$A_k(\theta) = \int d\vec{r}' \, e^{-i\vec{k}_k\cdot\vec{r}'_k} \, V_{k0}(r') \, e^{i\vec{k}_0\cdot\vec{r}'_0} \,. \qquad \text{(A25)}$$

In the case of collective excitation of a vibrational state, the interaction potential is again given by (A23). For simplicity it is convenient to take a zero range interaction.*

$$V_{k0} \longrightarrow V_{k0}(\vec{r}') \, \delta(\vec{r}'_k - \vec{r}'_0) \,. \qquad \text{(A26)}$$

In addition a square well potential will be assumed.

$$f(r) = 1 \,, \quad r < R$$
$$= 0 \,, \quad r > R \,. \qquad \text{(A27)}$$

Then the derivative in (A23) becomes

* Used in the DWB approximation also

$$\frac{\partial}{\partial r'} f(r') = -\delta(r'-R). \tag{A28}$$

Putting $\vec{r}_k' = \vec{r}_0' = \vec{r}'$ according to (A26) and using (A21), (A23) and (A28) the scattering amplitude (A25) becomes

$$A_k(\theta) = -VR\beta_\lambda/(2\lambda+1)^{1/2} \times \sum_\mu' \int d\vec{r}' e^{i(\vec{k}_o-\vec{k}_k)\cdot\vec{r}'} \delta(r'-R)\, Y_{\lambda\mu}^*(\vec{r}'). \tag{A29}$$

Now using the expansion for a plane wave in the direction of $\vec{q}$ where

$$\vec{q} = \vec{k}_o - \vec{k}_k \tag{A30}$$

is the momentum transfer,

$$e^{i\vec{q}\cdot\vec{r}'} = 4\pi \sum_{s=0}^{\infty} \sum_{t=-s}^{s}{}' i^s j_s(qr') \times Y_{st}^*(\vec{q}(\vec{r}'))\, Y_{st}(\Omega'). \tag{A31}$$

Substituting this expression in (A29) and integrating over r' gives

$$A_k(\theta) = -[4\pi VR^3\beta_\lambda/(2\lambda+1)^{1/2}] \sum_{st}' i^s j_s(qR) \times \sum_\mu' \int d\Omega'\, Y_{st}^*(\vec{q}(\vec{r}'))\, Y_{st}(\Omega')\, Y_{\lambda\mu}^*(\Omega'). \tag{A32}$$

Now choose the z' axis along $\vec{q}$ and note that the integration over Ω' requires that $S = \lambda$ and $t = \mu$.

$$\delta_{s\lambda}\delta_{t\mu} \sum_{\mu st}' Y_{st}^*(\vec{q}(\vec{r}')) = \sum_\mu' Y_{\lambda\mu}^*(Z') = Y_{\lambda 0}^*(Z') = [(2\lambda+1)/4\pi]^{1/2}. \tag{A33}$$

Thus the scattering amplitude becomes

$$A_k(\theta) = -4\pi V R^3 \beta_\lambda i^\lambda j_\lambda(qR), \quad \text{(A34)}$$

and the PWB cross section for excitation of a collective vibrational state in the limit of a zero range surface interaction is from (A11)

$$\left(\frac{d\sigma}{d\Omega}\right)_k = \frac{M_o M_k}{(2\pi\hbar^2)^2} \frac{k_k}{k_o} \times 4\pi V^2 R^6 \beta_\lambda^2 \left| j_\lambda(qR) \right|^2 . \quad \text{(A35)}$$

It is fairly easy to show that the same expression is obtained in the case of rotational excitation of a nucleus having a permanent deformation .

d) Summary

It has been shown that the Schroedinger equation for a two body scattering system can be expanded in terms of two complete sets of wave functions. One set describes the internal motion of the target nucleus. For example, shell model wave functions would be a convenient choice for this set. The other describes the relative motions of the two bodies. Optical model wave functions are the usual choice for the latter set with each optical wave function corresponding to a particular state of motion of the target system.

An approximate solution called the distorted wave Born (DWB) solution has been found for the inelastic scattering amplitude in terms of the two sets of wave functions.

In the special case of a strongly excited collective state it has been shown that the inelastic scattering amplitude depends only on the multipolarity of the transition, the optical model wave functions and a collective model parameter, β_λ, and is independent

of the type of nuclear wave functions used in the development of the DWB solution. In order to use this result to gain information about a specific nucleus it is only necessary to use the optical model to fit the elastic scattering data, then to calculate the DWB differential scattering cross section using the optical parameters found in fitting the elastic data. The value of the parameter, β_λ, is then varied to adjust the magnitude of the DWB cross section until it gives the best fit to the experimental data. The value of β_λ found in this way represents a measure of the collectiveness of the excited state. It is the only information about the excited state which can be extracted from the DWB solution.

Finally, a complete solution has been found for the excitation of a vibrational state using the plane wave Born (PWB) approximation.

APPENDIX B

RELATION BETWEEN β_λ AND THE ELECTROMAGNETIC TRANSITION PROBABILITY

The deformation parameter β_λ appropriate to a one phonon collective transition for an even-even nucleus having a sharp radius R_0 can be expressed in terms of the corresponding reduced electric multipole probability $B(E\lambda)$ [59]

$$B(E\lambda) = \left(\frac{3}{4\pi} Ze R^\lambda\right)^2 \beta_\lambda^2/(2\lambda+1) \qquad (B1)$$

where Ze is the nuclear charge and β_λ is a permanent deformation parameter in the case of rotational excitation or is given by equation (A21) in the case of a vibrational excitation. The reduced transition probability is in turn related to the mean lifetime τ of the collective state by

$$B(E\lambda) = \frac{\hbar}{8\pi\tau} \frac{\lambda[(2\lambda+1)!!]^2}{(\lambda+1)} \left[\frac{\hbar c}{Q}\right]^{2\lambda+1} \qquad (B2)$$

where $(2\lambda+1)!! = 1\cdot3\cdot5\cdot \ldots \cdot(2\lambda+1)$. Thus β_λ can be calculated if the mean lifetime is measured.

The relation (B1) can also be used in the case of a diffuse nuclear surface of given shape. To do this one can calculate a set of equivalent sharp radii r_λ which give the same multipole moments as those obtained for the diffuse surface. Such calculations have been done by Owen and Satchler [44] for nuclei having charge distributions given by

$$\rho(r) = \rho_o (e^x + 1)^{-1} \qquad (83)$$

where $x = (r - R_0)/a$). This expression will be recognized as having the same form of radial distribution as the real part of the optical potential (chapter II). However, the parameters a and R_0 which are appropriate here are not the parameters of the nucleon distribution but rather are those found for the charge distribution in the electron scattering experiments [41,42,43]. The latter are slightly smaller.

Transition probabilities are often expressed in terms of the extreme single particle estimates of Weisskopf which are estimates based on the movement of a single proton from a $j = l + \frac{1}{2}$ to a $j = \frac{1}{2}$ level. For electric multipole radiation of order $\lambda = 1$,

$$B(E\lambda)_{SP} = \frac{1}{4\pi}\left(\frac{3e}{\lambda+3}\right)^2 R_o^{2\lambda} . \qquad (84)$$

A single particle deformation parameter $\beta_\lambda(SP)$, that represents the collective deformation which would result in the same transition probability given by (84), can be defined by equating equations (81) and (84).

$$\beta_\lambda(SP) = \left[\frac{4\pi(2\lambda+1)}{(\lambda+3)^2 Z^2}\right]^{1/2}$$

$$= 1.653/Z \quad \text{for } \lambda = 3 . \qquad (85)$$

APPENDIX C

ELECTRONIC CIRCUITS USED IN THE TIME OF FLIGHT MEASUREMENTS

The circuits which were used for the time of flight measurements are shown in figures 23 to 26. They are basically the same as those designed by Fraser and Tomlinson[23] although there are many minor differences in the two systems.

The limiting preamplifier (figure 23) operates on the last dynode pulse of the photomultiplier and produces a 4 volt positive output pulse, more than 200 ns wide with a rise time of about 2.5 ns. The value given for the base resistor of the first transistor is nominal. It should be adjusted in order to put the operating point of the transistor in the region of highest gain-bandwidth product.

The TAC circuit (figure 24) operates on the 4 volt pulses of the limiting preamplifiers and produces a negative going output pulse of 0 to 5 volts amplitude depending on the time interval between the start and stop pulses. The time range covered is about 200 ns.

The clipper and fast coincidence unit (figure 25) also operates on the limiting preamplifier pulses. It produces positive and negative output pulses which are nominally one volt high.

The compensation circuit (figure 26) operates on the TAC output signal and a control pulse which should be positive and less than 20 volts high. The net gain of the circuit is somewhat less than one.

Figure 23: Limiting preamplifier circuit.

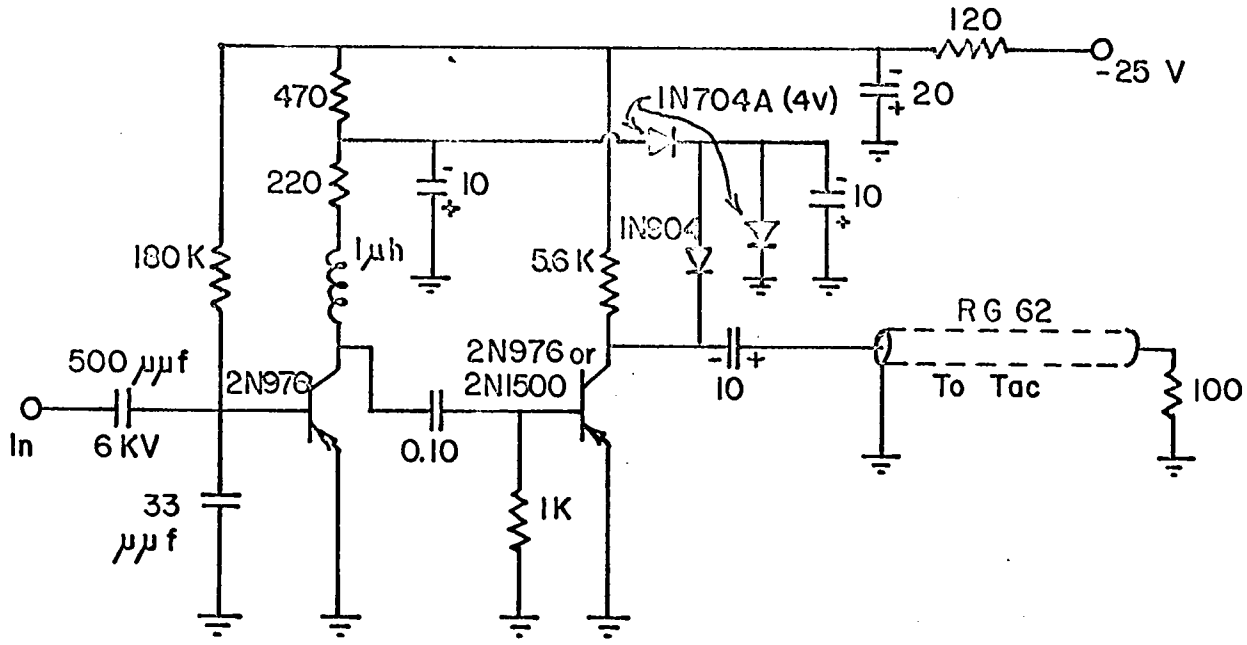
120
-25 V
470
IN704A (4v)
20
220
10
10
1 μh
180 K
IN904
5.6 K
RG 62
500 μμf
2N976
2N976 or
2N1500
10
To Tac
100
In
6 KV
0.10
33
μμf
1K

Figure 24: Time to amplitude converter (TAC) circuit.

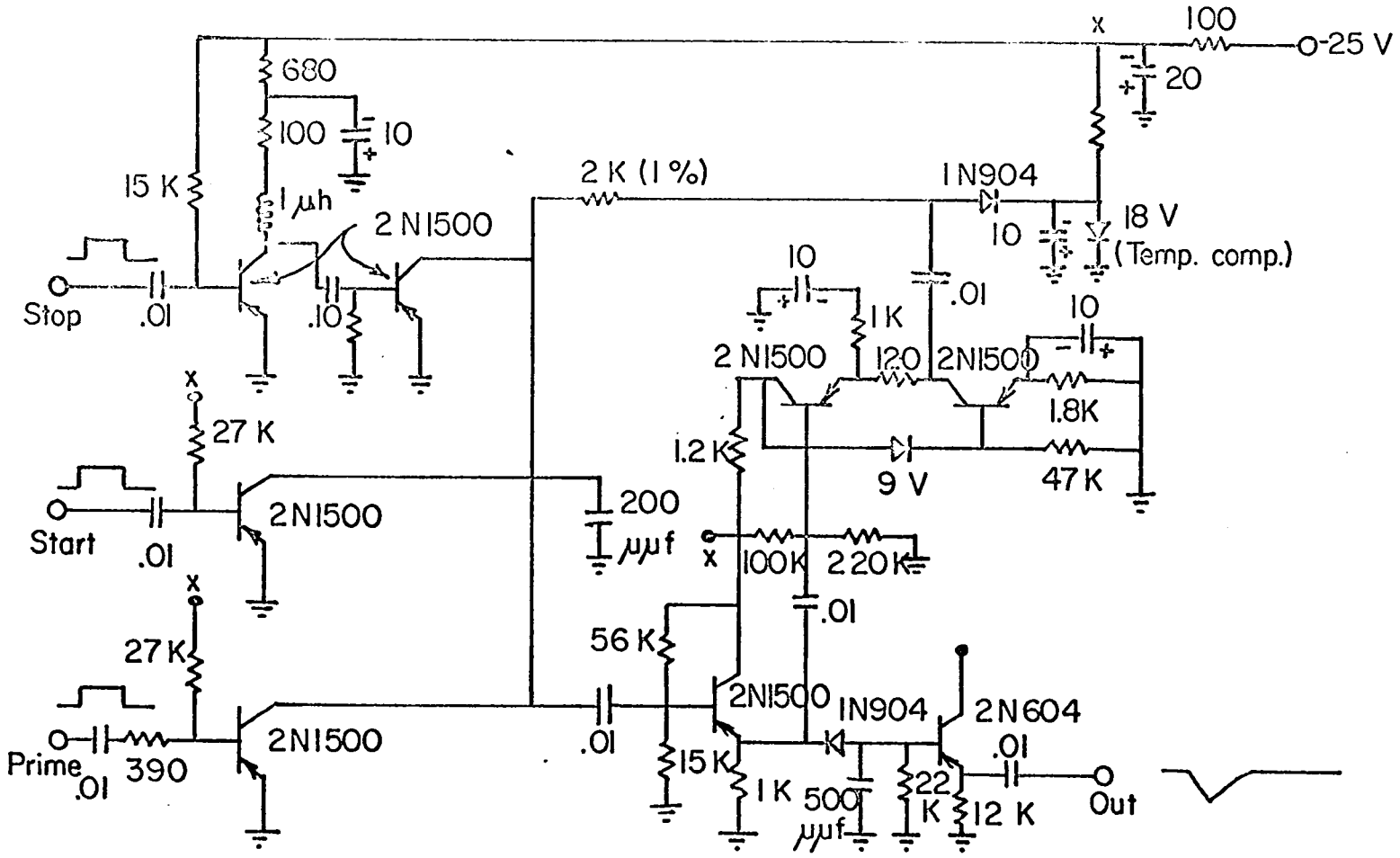
680
100
10
15 K
1 μh
2 N1500
Stop
.01
.10
2 K (1 %)
1 N904
10
18 V
(Temp. comp.)
x
100
-25 V
20
.01
10
1 K
2 N1500
120
2N1500
10
1.8K
1.2 K
9 V
47 K
27 K
2N1500
Start
.01
200
μμf
x
100K
220K
.01
27 K
56 K
2N1500
2N1500
Prime
.01
390
.01
15 K
1 K
1N904
500
μμf
2N604
.01
22
K
12 K
Out

Figure 25: Clipper and fast coincidence unit.

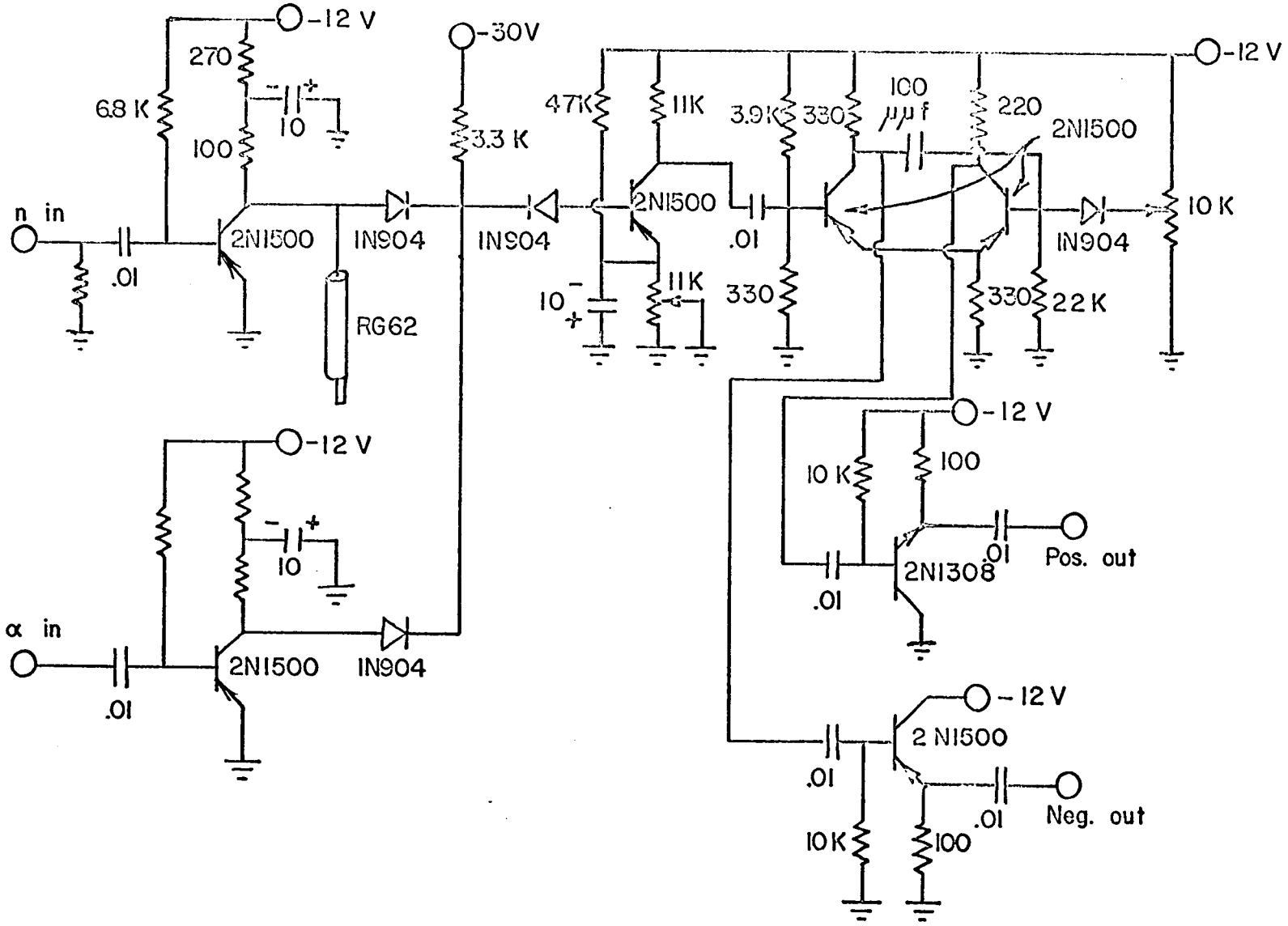
-12 V
270
6.8 K
100
10
n in
.01
2N1500
IN904
RG62
-30V
3.3 K
IN904
47K
11K
2N1500
10
11K
.01
3.9K
330
330
100 µµf
220
2N1500
IN904
10 K
330
22 K
-12 V
-12 V
α in
.01
2N1500
IN904
10
-12 V
10 K
100
.01
Pos. out
2N1308
.01
-12 V
2 N1500
.01
.01
Neg. out
10K
100

Figure 26: Compensation circuit.

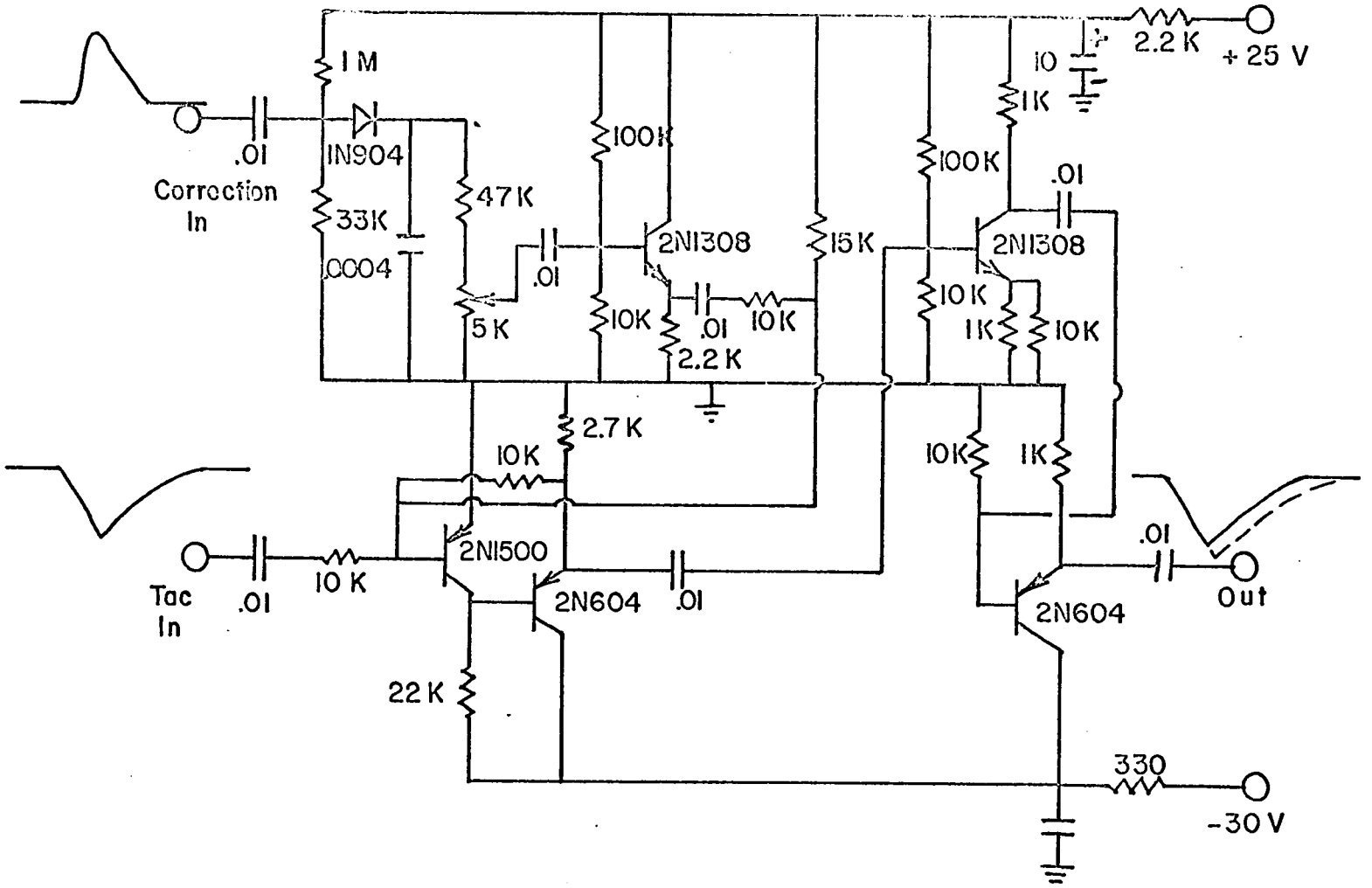
1 M
.01
Correction In
IN904
33K
.0004
47K
5K
.01
100K
2N1308
10K
.01
10K
2.2K
15K
2.7K
10K
2N1500
2N604
.01
10 K
Tac In
.01
22K
100K
10
1K
2.2 K
+ 25 V
.01
2N1308
10K
1K
10K
10K
1K
.01
2N604
Out
330
-30 V

BIBLIOGRAPHY

1) V.F. Weisskopf, Physics Today 14 no. 7 (1961) 18

2) A.M. Lane and E.D. Pendlebury, Nuc. Phys. 15 (1960) 39

3) S. Fallieros and R.A. Farrell, Phys. Rev. 116 (1960) 660 (see also reference 1)

4) A.E. Litherland, J.A. Kuehner, H.E. Gove, M.A. Clark and E. Almqvist, Phys. Rev. Lett. 7 (1961) 98

5) J.P. Elliott and M. Harvey, Proc. Roy. Soc. Lon. A272 (1963) 557

6) B.L. Cohen and A.G. Rubin, Phys. Rev. 111 (1958) 1568

7) W.T. Pinkston and G.R. Satchler, Nuc. Phys. 27 (1961) 270

8) N. Austern in "Fast Neutron Physics, Part II" ed. by J.B. Marion and J.L. Fowler (Interscience, New York, 1963)

9) H. Feshbach, C.E. Porter and V.F. Weisskopf, Phys. Rev. 96 (1954) 448

10) D.M. Chase, L. Wilets and A.R. Edmonds, Phys. Rev. 110 (1958) 1080

11) B. Buck, Phys. Rev. 130 (1963) 712

12) F. Perey and G.R. Satchler, Phys. Lett. 5 (1963) 212

13) D.M. Chase, Phys. Rev. 104 (1956) 838

14) E. Rost and N. Austern, Phys. Rev. 120 (1960) 1375

15) J.S. Blair, Phys. Rev. 115 (1959) 928

16) G. Igo and R.M. Thaler, Phys. Rev. 106 (1957) 126

BIBLIOGRAPHY (continued)

17) K. Matsuda, Nuc. Phys. 33 (1962) 536

18) G.R. Satchler, Proc. Phys. Soc. A68 (1955) 1037

19) C.A. Levinson and M.K. Banerjee, Ann. Phys. (New York) 2 (1957) 499

20) M. Nomoto, Phys. Rev. 127 (1962) 1693

21) G.K. O'Neill, Phys. Rev. 95 (1954) 1235

22) G.C. Neilson, W.K. Dawson, F.A. Johnson and J.T. Sample, Suffield technical paper no. 167, Defense Research Board of Canada

23) J.S. Fraser and R.B. Tomlinson, Atomic Energy of Canada Limited report no. AECL-3119 (unpublished)

24) M. Gettner and W. Selove, Rev. Sci. Inst. 31 (1960) 450

25) B.V. Rybakov and V.A. Siderov, "Fast Neutron Spectroscopy", Supplement No. 6, Sov. J. of Atomic Energy, 1958, English translation (Consultents Bureau, New York)

26) I; D.A. Bromley, H.E. Gove, J.A. Kuehner, A.E. Litherland and E. Almqvist, Phys. Rev. 114 (1959) 758
II; J.A. Kuehner, A.E. Litherland, E. Almquist, D.A. Bromley and H.E. Gove, Phys. Rev. 114 (1959) 775

27) C. Glavina, M.Sc. Thesis, University of Ottawa, Ottawa, Ontario (unpublished)

28) D.J. Hughs, B.A. Magurno and M.K. Brussel, "Neutron Cross Sections", Brookhaven National Laboratory report BNL 325, Sec. Ed., Supp. no. 1

29) N.N. Flerov and V.M. Talyzin, Atomic Energy, U.S.S.R. (English translation) 4 (1956) 617

BIBLIOGRAPHY (continued)

30) R.W. Bauer, J.D. Anderson and L.J. Christensen, Nuc. Phys. 47 (1963) 241

31) M.H. MacGregor, W.P. Ball and R. Booth, Phys. Rev. 108 (1957) 726

32) D. Blum, P. Barreau and J. Bellicard, in "Direct Reactions and Nuclear Reaction Mechanisms", (Padua Conference) ed. by E. Clementel and C. Villi (Gordon and Breach, New York)

33) P.M. Endt and C. Van der Leun, Nuc. Phys. 34 (1962) 1

34) W.G. Cross and R.G. Jarvis, Nuc. Phys. 15 (1960) 155

35) J.P. Conner, Phys. Rev. 109 (1958) 1268

36) F.E. Bjorklund and S. Fernbach, Phys. Rev. 109 (1958) 1295

37) R.L. Clarke and W.G. Cross, Nuc. Phys. 53 (1964) 177

38) W. Hauser and H. Feshbach, Phys. Rev. 87 (1952) 366

39) S. Kobayashi, Jour. Phys. Soc. Japan 15 (1960) 1164

40) M.A. Melkanoff, S.A. Moszkowski, J. Nodvik and D.S. Saxon, Phys. Rev. 101 (1956) 507

41) B. Hahn, D.G. Ravenhall, and R. Hofstadter, Phys. Rev. 101 (1956) 1131

42) R.H. Helm, Phys. Rev. 104 (1956) 1466

43) R. Hofstadter, Ann. Rev. Nuc. Sci. 7 (1957) 231

44) L.W. Owen and G.R. Satchler, Nuc. Phys. 51 (1964) 155

45) N.K. Glendenning, Phys. Rev. 114 (1959) 1297

BIBLIOGRAPHY (continued)

46) R.H. Bassel, G.R. Satchler, R.M. Drisko and E. Rost, Phys. Rev. 128 (1962) 2693,
E. Rost, Phys. Rev. 128 (1962) 2708

47) R.B. Day and D.A. Lind, Bull. Am. Phys. Soc. 2 (1957) 32

48) W.M. Deuchars and D. Dendy, Proc. Phys. Soc. LXXV (1960) 855

49) F. Ajzenberg-Selove and T. Lauritsen, Landolt-Bornstein, Group I, 1 (1961) 1-54

50) H.E. Gove and A.R. Rutledge, Chalk River report CRP 755 (unpublished)

51) W.F. Miller and W.J. Snow, Rev. Sci. Inst. 31 (1960) 39

52) D.J. Rowe, A.B. Clegg, G.L. Salmon, and D. Newton, in "Proceedings of the Rutherford Jubilee International Conference", ed. by J.B. Birks (Heywood, London, 1961)

53) D.H. Wilkinson, B.J. Toppel, and D.E. Alburger, Phys. Rev. 101 (1956) 673

54) F.G.J. Perey, Ph.D. Thesis, University of Montreal, Montreal, Quebec

55) K. Yagi, H. Ejiri, M. Furukawa, Y. Ishizaki, M. Koike, K. Matsuda, Y. Nakajima, I. Nonaka, Y. Saji, E. Tanaka and G.R. Satchler, Phys. Lett. 10 (1964) 186

56) G.R. Satchler, R.H. Bassel, and R.M. Drisko, Phys. Lett. 5 (1963) 256

57) A.P. Stamp and J.R. Rook, Nuc. Phys. 53 (1964) 657

BIBLIOGRAPHY (continued)

58. P.M. Morse and H. Feshbach, "Methods of Theoretical Physics", (McGraw Hill, New York)

59. A. Bohr and B.R. Mottelson, Dan. Mat. Fys. Medd. 27 no. 16 (1953);
K. Alder, A. Bohr, T. Huus, B. Mottelson and A. Winther, Rev. Mod. Phys. 28 (1956) 523

VITA

NAME: Wallace John McDonald

BORN: Lethbridge, Alberta, Canada, 1936

EDUCATED:

Primary — Taber Public School, Taber, Alberta, 1941-1950

Secondary — Taber High School, Taber, Alberta, 1950-1953
Red Deer Composite High School, Red Deer, Alberta, 1953

University — University of Saskatchewan,
Saskatoon, Saskatchewan, 1955-1961

Course — Physics

Degrees — B.Sc. (Honours) 1959
M.Sc. 1961

PUBLICATIONS

The $Mg^{24}(\gamma,n)\,Mg^{23}$ Reaction, J.D. King and W.J. McDonald, Nuc. Phys. 19 (1960) 94.

The Gamma Neutron Cross Section for F^{19}, J.D. King, R.N.H. Haslam and W.J. McDonald, Can. J. Phys. 38 (1960) 1069.

Note on the Reaction $P^{31}(\gamma,n)\,P^{30}$, W.J. McDonald, E. Buchholtz and R.N.H. Haslam.

The Scattering of 14.1 MeV Neutrons by Ca^{40}, W.J. McDonald and J.M. Robson, Nuc. Phys. (to be published).